Design and Implementation of A Novel Single-Phase Switched Reluctance Motor Drive System

By:
Amanda Martin Staley

Thesis submitted to the Faculty of the Virginia Polytechnic Institute and State University in partial fulfillment of the requirements for the degree of

Master of Science

in

Electrical Engineering

Approved:

Dr. Krishnan Ramu, Chair

Dr. Lamine Mili

Dr. Hugh VanLandingham

August 21, 2001
Blacksburg, Virginia

Keywords: Single Phase Switched Reluctance Motor, Auxiliary Windings, Reliable Starting, Minimum Cost, Minimum Component Control

Design and Implementation of A Novel Single-Phase Switched Reluctance Motor Drive System

By:
Amanda Martin Staley

(Abstract)

Single phase switched reluctance machines (SRMs) have a special place in the emerging high-volume, low-cost and low-performance applications in appliances and also in high-speed low-power motor drives in various industrial applications. Single phase SRMs have a number of drawbacks: low power density as they have only 50% utilization of windings, lack of self-starting feature unless otherwise built in to the machine, most of the times with permanent magnets or sometimes with distinct and special machine rotor configurations or additional mechanisms. Many of these approaches are expensive or make the manufacturing process more difficult. In order to overcome such disadvantages a method involving interpoles and windings is discussed in this research. Also, a new and novel converter topology requiring only a single switch and a single diode is realized.

This research tests the concepts and feasibility of this new single-phase SRM motor topology and converter in one quadrant operation. The converter electronics and a simple minimum component, minimum cost analog converter are designed and implemented. The entire system is simulated and evaluated on its advantages and disadvantages. Simple testing without load is performed.

This system has a large number of possibilities for development. Due to its lightweight, compact design and efficient, variable high-speed operation, the system might find many applications in pumps, fans, and drills.

Acknowledgements

There are numerous people I must thank that have helped me through the course of my graduate studies. I would like to express my deepest gratitude to my advisor, Dr. Krishnan Ramu. Without his constant support, this research would never have come to fruition. Also, I would like to thank Dr. Lamine Mili and Dr. Hugh VanLandingham for taking the time to be part of my examination committee.

I would also like to thank my family and my friends. Their constant prodding helped me reach the heights I have found today. I would especially like to thank those that I worked with at MCSRG, particularly Praveen Vijayraghavan, Phillip Vallance, and Ajit Bhanot. Also, I would like to thank my parents, Brenda and David Martin, my brother, Kevin Martin, and my husband, Shaun Staley. They had faith in me, even when I did not.

Finally, I would like to express my appreciation to the Via Family for supporting my research and studies through the Bradley Fellowship. Without this funding, the research in this area might not have been possible.

Table of Contents

List of Figures

List of Tables

List of Symbols

i^* – Current Command / Current Reference

i_f – Total Current Feedback

i_{af} – Total Amplified Current Feedback

i_m – Current Feedback from Sensing Resistor 1 (Main Current after the switch)

i_a – Current Feedback from Sensing Resistor 2 (Auxiliary Current at snubber capacitor node)

V_{ac} – AC Mains Voltage

V_{dc} – DC Link Voltage

w^* – Speed Reference / Speed Command

w_f – Speed Feedback

Chapter 1. Introduction

1.1 History of the Switched Reluctance Machine and Principles of its Operation

Most people believe that switched reluctance motors (SRMs) is new to the machine scene. In actuality, SR machines have been around since 1838. But, the effective and efficient operation of SR machines has only recently been possible with the advent of power electronic devices. With the dropping prices of devices and its increasing popularity, switched reluctance is beginning to create a foothold in industry.

In order to understand the operation of a SR machine, we can look to its name. The machine operates on the tendency for its rotor to move to a position where the reluctance is minimized. SR motors also go by another name, Electronically Commutated Machines. These two names fully explain the motor's operation. Stator windings are energized at specific times to change the rotating magnetic field to move rotor poles to a position of minimized reluctance, or equivalently maximized inductance. This position is where the rotor pole is aligned with the energized stator pole. Movement in different directions and at different speeds can be achieved by exciting stator windings in a particular sequence with a particular timing.

SR motors have several distinct advantages over most motors including induction motors.

- High efficiency - 80% efficiency depending on the application
- Salient rotor and stator poles and no rotor windings (singly excited) – reduced operation and material costs
- A speed range that rivals induction motors – introduction of high speed switching devices
- Windings are energized and de-energized only when needed – decreased power consumption
- Fault tolerant operation – independent windings
- High starting torque
- Low losses except switching losses

On the other hand, there are some disadvantages associated with switched reluctance.

- Requires knowledge of rotor position – usually must include sensors which increase cost

- Can require sophisticated acoustic noise control due to vibrations inherent with operation
- Sometimes requires high cost electronic components for control and power conversion
- Application needs to be unaffected by torque ripple or control is required

To date, work has been done on multi-phase switched reluctance drives, but single-phase motors have been overlooked. For low power, low performance applications, single-phase SRMs are a perfect match because they have: simplicity in construction, robustness, compactness, low cost, and high efficiency. Single-phase machines have even further reduced costs since the number of switching devices is decreased. The architecture of a single phase SRM can also be simplified from the poly-phase SRM to involve a smaller number of poles and windings, decreasing cost in the manufacturing process. However, they also have the same disadvantages of polyphase SRMs such as the need for rotor position information. Also, single-phase SRMs have a large problem in that they do not have reliable starting capability. This roadblock to effective operation of a single-phase SR motor is the motor's tendency to lock in a position that does not allow further rotation. If the rotor is in a position of minimal reluctance to begin with, it will be incapable of producing torque; therefore, making it necessary to restart and reinitialize the motor to attempt another start.

1.2 Previous Art of Single-Phase Switched Reluctance Motor Drives

Most of the prior art is limited to machine design and converter topologies. In addition to these topics, some patents are included that discuss the issue of reliable starting. A review of the current literature follows.

Chan [1] in 1987 proposed a novel drive involving a machine configuration, converter design, and a control circuit. Two converter-control schemes are evaluated. The first involves a triac chopper with a synchronizing circuit with position sensor information. This circuit uses a flip flop to fire the transistor when the state is changed by the input and a clock generated by a zero crossing detector attached to a 15 V AC source. The second scheme has become well known. It involves an asymmetric bridge converter with a PWM control circuit. Parking magnets are used to ensure that the rotor stops in a position that will allow restarting. This design did not attempt to eliminate devices to allow for a lower cost solution.

In [2], a new 4 rotor pole and 4 stator pole (4:4) SRM is presented. This configuration is novel in that while retaining the advantages of a 4:4 machine, they have reduced the core length and the copper loss to near that of a 2:2 machine. This is accomplished by using a 4:4 design but creating the flux pattern of a 2:2 machine by allowing a pole sequence of NNSS instead of NSNS. However, this machine has a drawback; the iron loss has been increased, and in order to address starting, the use of permanent magnets has been introduced.

In [3], a novel machine design having both a radial and an axial air gap is disclosed. The rotor and the stator have been stacked with two different sets of laminations. This design increases the maximum inductance allowing for increased torque. This design does not address the issue of starting.

In [4], an asymmetric half bridge converter is fitted with a voltage boosting circuit. Its advantages include reducing the rise and fall times of the motor current and allowing for a higher mean current without a higher supply voltage. Also, the mean output power is increased with the addition of this boost circuit, but the capacitor must be sized appropriately to allow for maximum advantage. The primary disadvantage of this design is the number of semiconductor devices that is required. Three diodes and two switches are required in addition to the boost capacitor.

In [5], a novel power converter is introduced for single-phase SR motors. This topology is a modification of a series DC link voltage boosting converter in that it requires one less diode. This converter's advantages include great control over turn on and turn off voltage boosting and a reduction in the number of required devices. Its disadvantages include the negative voltage applied is reduced leaving less voltage to reduce the current in the windings and the requirement of two switches.

Barnes and Pollock [6] introduce a converter selection process. This paper realizes the need to reduce costs for lower power drives and thereby select the converter that is optimal for each specific application. Several different converter choices are discussed.

Single-phase SRMs inherently lack self-starting capability. The motor has a tendency to lock in a position that does not allow further rotation while beginning the starting procedure. If the rotor is in a position of minimal reluctance to begin with, i.e., when the stator and rotor poles are perfectly aligned, it will not be able to produce a torque to turn; therefore, making it necessary to provide an externally induced means of starting. Only a few designs have been realized to help the single-phase motor overcome this difficulty and they are briefly described in the following.

One such design is disclosed in [7]. This patent discloses a mechanism that engages the rotor by means of teeth on the rotor shaft to the teeth on a starting shaft to allow for starting shown in figure 1.1. Once engaged, the starting shaft sets the rotor into motion and then drops into a holding position around the rotor shaft. The problem with this design is that it allows for further mechanical problems that could be associated with the mechanism. Also, this will increase the possibility of friction problems, which would otherwise not be an issue.

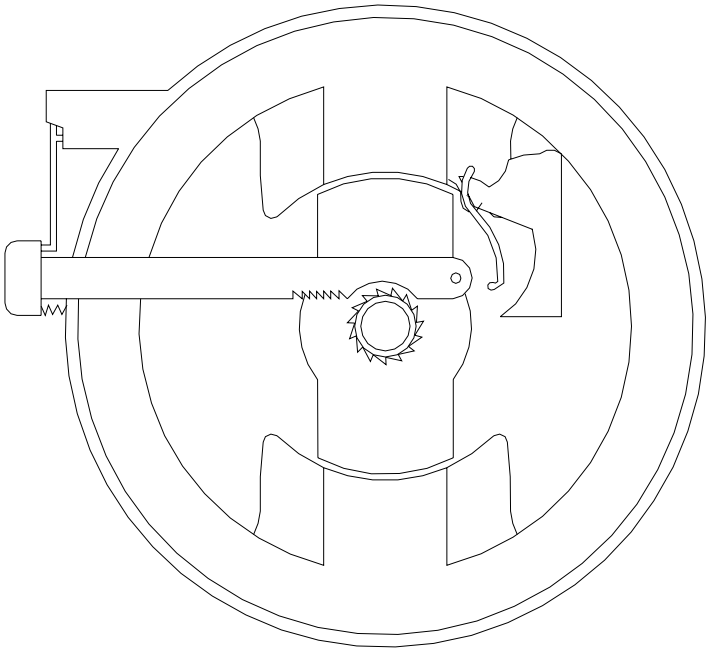

Figure 1.1 – Single-Phase SRM Involving a Holding Mechanism for Reliable Starting

One other design is disclosed in [8] which a vane is attached to the shaft of the motor shown in figure 1.2. This vane includes permanent magnets and sensors that help align the rotor in an appropriate position for reliable starting. Issues with this design also include further

mechanical problems and friction problems. Also, this vane adds to the size of the machine, which detracts from the machine's compactness and simplicity. Also, it adds to the total cost since the vane requires permanent magnets and sensors for proper operation. Another design involves the use of a parking magnet that is off center from the midpoint between the windings. This enables the rotor to be parked in a position of minimum inductance, i.e., at the completely unaligned position between the stator and rotor poles, thus enabling starting by energizing the stator winding. But it requires the use of a magnet increasing the manufacturing complexity and the cost of the machine significantly.

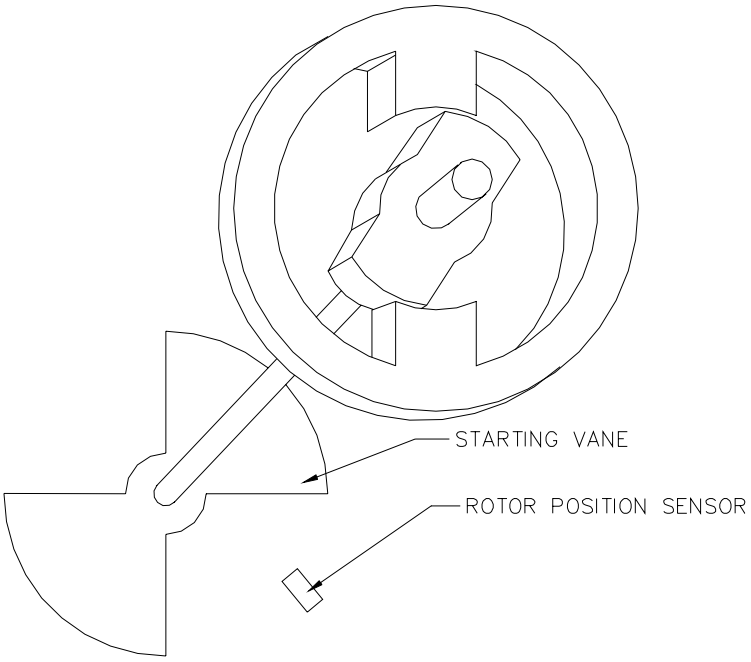

Figure 1.2 – Single-Phase SRM Involving a Vane for Reliable Starting

Another approach to this problem is to the shift a pole-pair [9]. The rotor poles of this machine have shoulders that allow for different air gaps, thus lending itself to a continuous variation of reluctance and hence to torque generation at all positions. This proposed technique involves the use of a shifted stator pole that has a parking permanent magnet attached as shown in figure 1.3. The reason for the shift is to eliminate the possibility of the locking the rotor into a stable detent (completely aligned) position. This technique includes permanent magnets that are undesirable in a low cost solution.

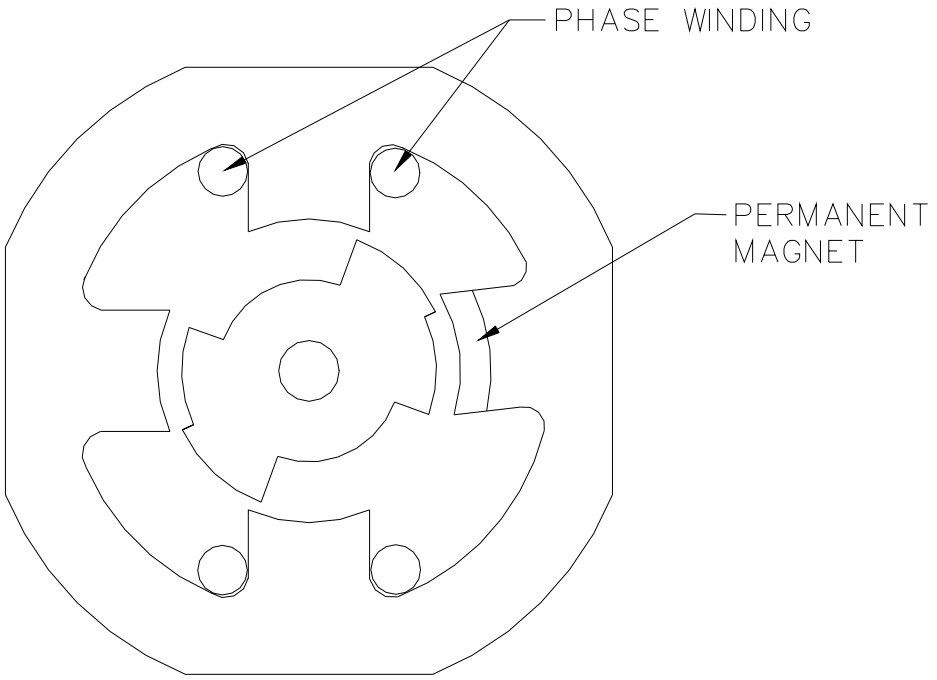

Figure 1.3 – Single-Phase SRM Involving Pole Shaping and Permanent Magnets for Starting

1.3 Objectives and Novel Concepts of Proposed Drive System

The designed drive system will be a variable speed drive that is capable of speeds up to 10,000 revolutions per minute with a power output of 100 Watts and an average torque output of 0.1 Newton-meters. The novel contributions of this thesis include electronic design of the converter and control circuitry, implementation of the proposed drive system, and experimental verification of operation. The research results presented here are also presented in [11].

1.4 Scope of System Design

This topic presents a vast array of possibilities for research, but in the interest of time, limitations must be placed on this thesis. This research is limited to system design including motor topology and converter selections in addition to the control system design. The analysis will include experimental verification and validation of results.

The control system design will be limited to energizing control of the machine, reliable starting, and variable speed operation control. Acoustic noise control is outside of the scope of this study.

1.5 Organization of Materials Presented

This thesis will be organized into chapters in the following method. Chapter two will present the motor topology and machine specifics. Discussion will include dimensions, machine torque and flux linkage versus position characteristics, and inductance measurements. Finite Element Analysis results will also be presented.

Chapter three will introduce the converter selection. In this section we will describe the purpose of the converter and its place in the system. Also, this section will evaluate the different converter topologies and the motivation behind the selection made. Advantages and disadvantages of the chosen strategy will be reviewed.

Chapter four will present the requirements of the control system and the approaches taken to meet the goals set. The electronics and components used will be discussed, and the details of the construction of the subsystem and connection to the drive will be outlined. Advantages and disadvantages of the methodology used will be discussed.

Chapter five presents and analyzes the results. Since it is the intention of this project to construct a fully operational prototype, experimental results will be presented.

Finally, chapter six will summarize the project and provide results and key conclusions of this research work. Advantages and limitations of the proposed system will be reviewed. Possible applications and recommendations for future related work will be submitted.

Chapter 2. Machine Configuration

2.1 Machine Description

2.1.1 Dimensions

The machine configuration used in this thesis was designed by Kartik Sitapati of Kollmorgen Custom Motor Drives and Dr. Krishnan Ramu of Virginia Tech. It is shown in figure 2.1 and, it has four stator poles, four rotor poles, and four auxiliary stator poles, which hereafter are referred to as interpoles; this machine is shortly referred to as a 4:4:4 design. Each stator pole is 25.5 millimeters (1.0039 inches) in width and has a radius of curvature of 36 degrees. The stator inner diameter is 74.5 millimeters (2.933 inches). The stator back iron diameter is 102 millimeters (4.0157 inches). The outer stator width is 75 millimeters (2.95276 inches). The rotor outer diameter is 73.8 millimeters (2.9055 inches). The rotor poles are slightly larger with a width of 26.5 millimeters (1.0433 inches) and a radius of curvature of 40 degrees. The rotor stack length is 18 mm (0.70866 inches). The rotor shaft diameter is 6.25 mm (0.24606 inches). The case of the machine is square with a side length of 135 millimeters (5.31496 inches). The stack length is 10 millimeters (0.3937 inches). The main purpose of the interpoles is to provide reliable starting. This is achieved by pulsing the interpole windings with a small current that will pull the nearest rotor poles to complete alignment with the interpoles. Note that in this position the rotor poles are completely unaligned with respect to the main stator poles. Then excitation of the main stator poles at this time will generate an air gap torque turning the rotor. Note that only one set of interpoles is involved for starting in one direction and therefore, at any time, only one set of interpoles is being used. The major advantages and disadvantages of the proposed machine configuration are derived below.

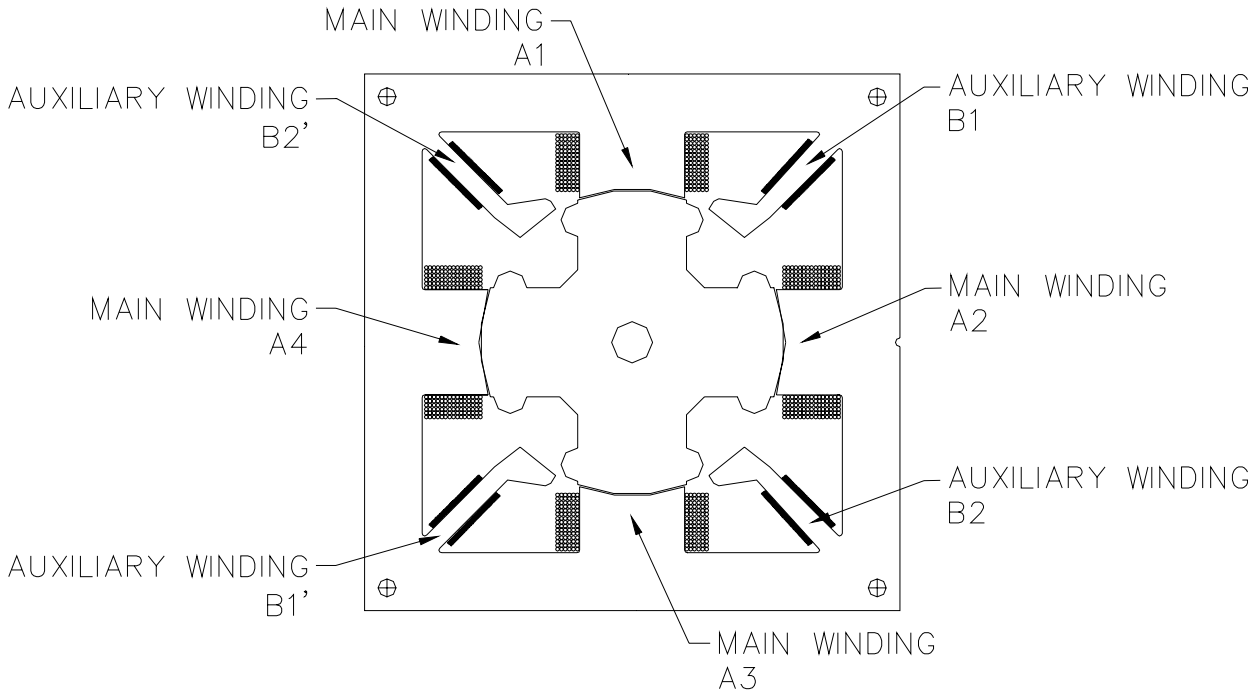

Figure 2.1 – Proposed machine configuration

Advantages include:

(i) Provides reliable self-starting capability at all rotor positions.

(ii) Provides starting capability in both directions unlike other single-phase SRM configurations and, therefore, this is the only single-phase configuration capable of true four-quadrant operation.

(iii) Does not use permanent magnets thus reducing the manufacturing complexity of the machine and cost.

(iv) The interpole winding can be used, in addition to self-starting, for probing to determine the rotor position or as an inactive phase.

(v) After starting, the interpoles need not be used for continuous operation of the machine as the main winding itself, and can be used for sensing the rotor position.

(vi) Since the interpole winding is only used for a small amount of time (during starting), it can be designed to have a very small volume of copper thereby reducing its cost. During the sensing part of the cycle, its current is very small even if its duty cycle is high and, therefore, a small copper volume design is adequate.

(vii) If necessary, the air gap torque can be augmented by using the interpole winding as another phase of a two-phase SRM or both the interpole windings can be used as other two phases of a three-phase SRM. This allows the fullest utilization of the electromagnetic capability of the machine. Many such modes of operation are possible with this unique SRM.

(viii) Sensing of induced emf in the interpole winding during the excitation of the main winding gives an indication of the mutual inductance and hence the rotor position. An alternative is to apply high frequency signal at low current to the interpole winding and measure its self-inductance from which the rotor positions can be estimated.

Disadvantages include:

(i) Interpole punchings and their windings and hence slightly higher cost of manufacturing.

(ii) Extra terminal connections for interpole windings and hence their unsuitability for applications involving hermetic sealing.

2.1.2 Power Statistics and Finite Element Analysis Results

The operating power is 100 Watts and its maximum speed is 10,000 revolutions per minute. The machine magnetic characterization can be derived by analytical or using finite element analysis (FEA) software. The latter approach is selected for the present study. All FEA results presented here are contributed by Kartik Sitapati. Sample results for only main winding and interpole winding excitations with the aligned main poles aligned are shown in figures 2.2 and 2.3, respectively.

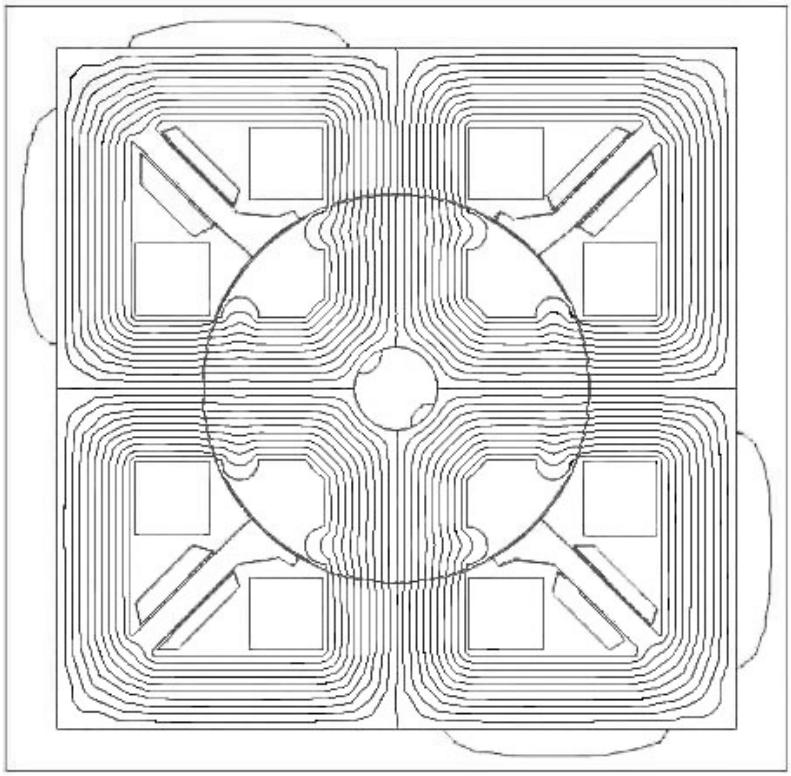

Figure 2.2 – FEA – Main Windings energized with 8 A DC

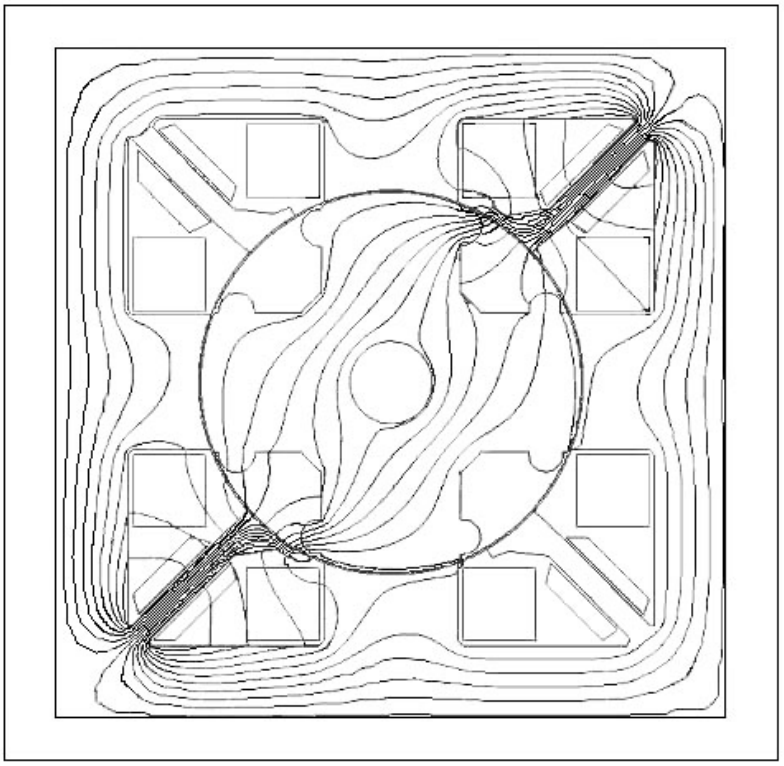

Figure 2.3 – FEA – Interpole pair #1 energized with 2 A DC

The flux in the aligned position for the main winding excitation is easier to determine analytically but for the unaligned position becomes very demanding as in the case of any other SRM. That is the reason for the use of FEA software for the analysis. It must be noted at this time that the FEA analysis was performed for a machine that had the same dimensions as the experimental prototype, but the stack length was 50 mm instead of 10 mm. Also, the number of turns for the main poles was 100 instead of the actual 92 turns. The number of turns for the auxiliary poles was 250 instead of the actual 205 turns. Accordingly, the graphs have been scaled in order to provide a clear view of the prototype's capabilities. The main pole calculations have been scaled by:

$$Prototype\ Mains = FEA\ Mains\left(\frac{10\ mm\ stack}{50\ mm\ stack}\right)\left(\frac{92\ turns}{100\ turns}\right)$$

The auxiliary pole calculations have been scaled by:

$$Prototype\ Interpoles = FEA\ Interpoles\left(\frac{10\ mm\ stack}{50\ mm\ stack}\right)\left(\frac{205\ turns}{250\ turns}\right)$$

Figure 2.4 shows the beginning of torque production of interpole 1 and that corresponds to unaligned position for the interpole but position of alignment for main poles.

Flux linkages for various rotor positions for main, and interpoles 1 and 2 are obtained by mechanizing the results from FEA and are shown in figure 2.5, for 8 A main winding current and 2 A of interpole winding current. These are the rated values for these windings. Air gap torques are extracted from the FEA results and are shown in figures 2.6 and 2.7 for main and interpole windings 1 and 2, respectively. The interpole torques are designed with a maximum of 0.04 N-m. The main windings produce a peak of 0.325 N-m but are required to produce only 0.1 N-m on average, which is sufficient for a fan type load under consideration. Therefore, from the figures 2.6 and 2.7, it is seen that the machine is capable of providing the required torque and performance.

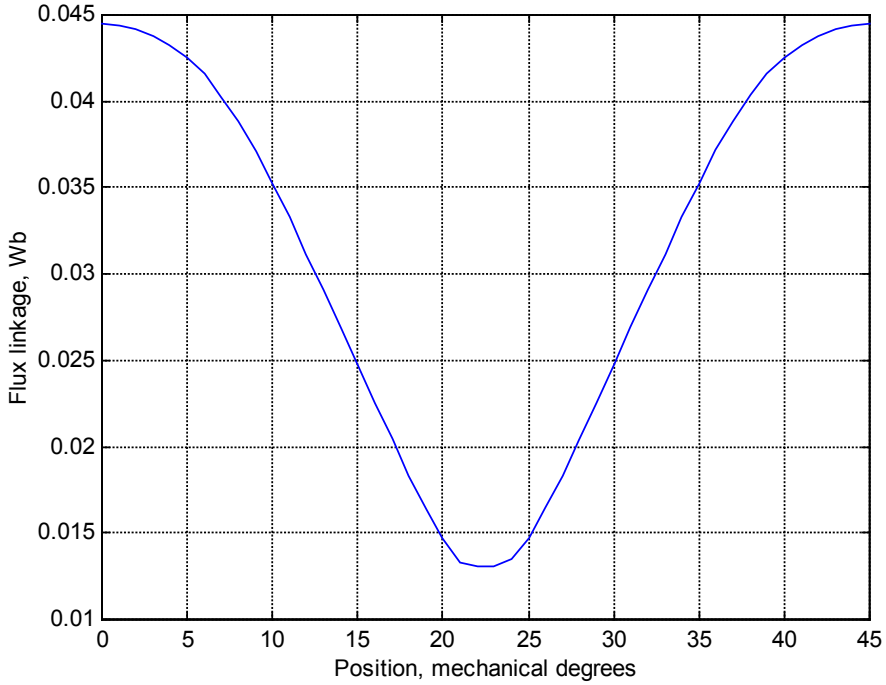

Figure 2.4 – Flux Linkage – Main windings energized

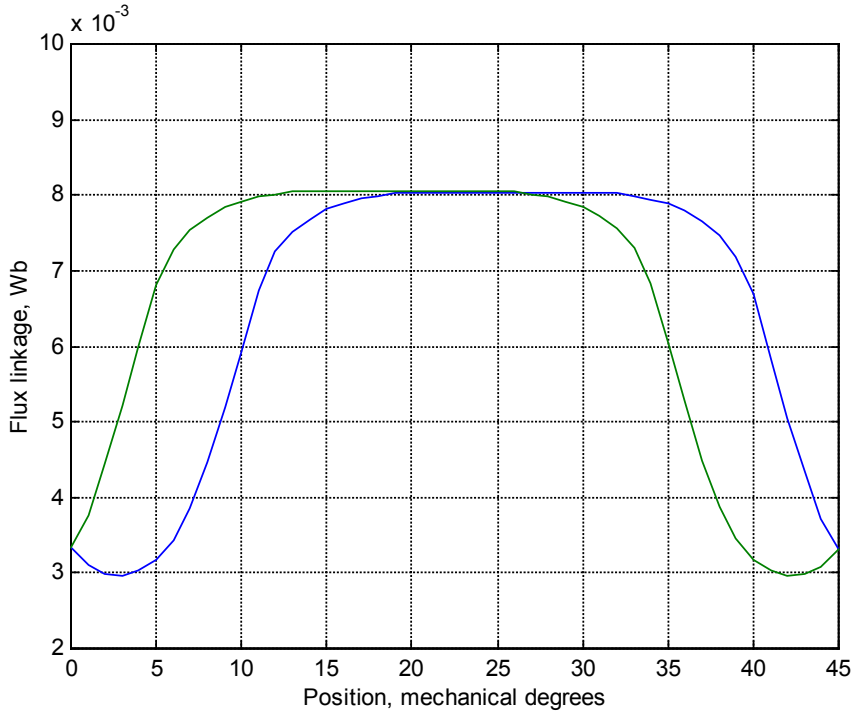

Figure 2.5 – Flux Linkage - Interpole pairs #1 and #2 energized

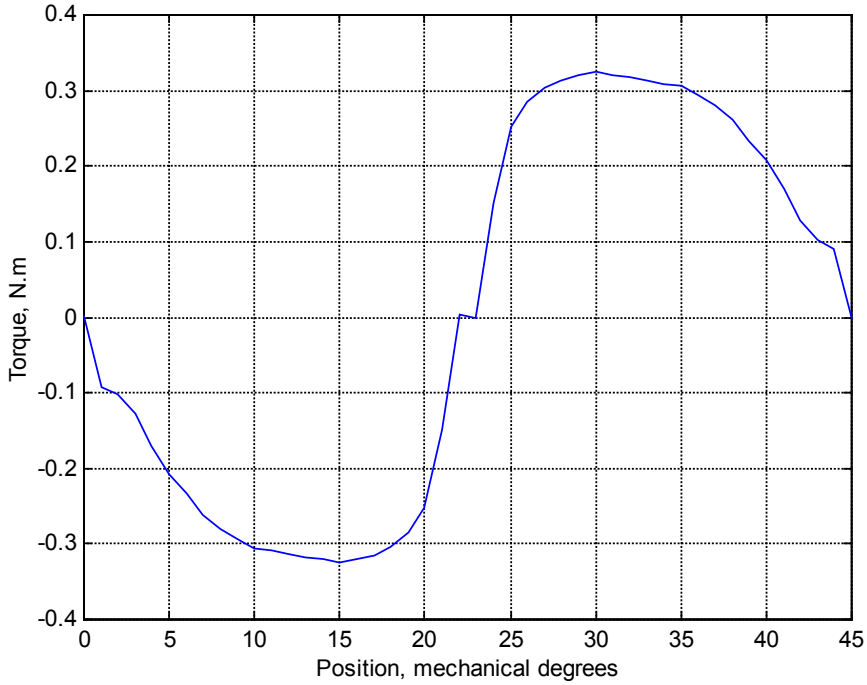

Figure 2.6 – Torque – Main Windings energized

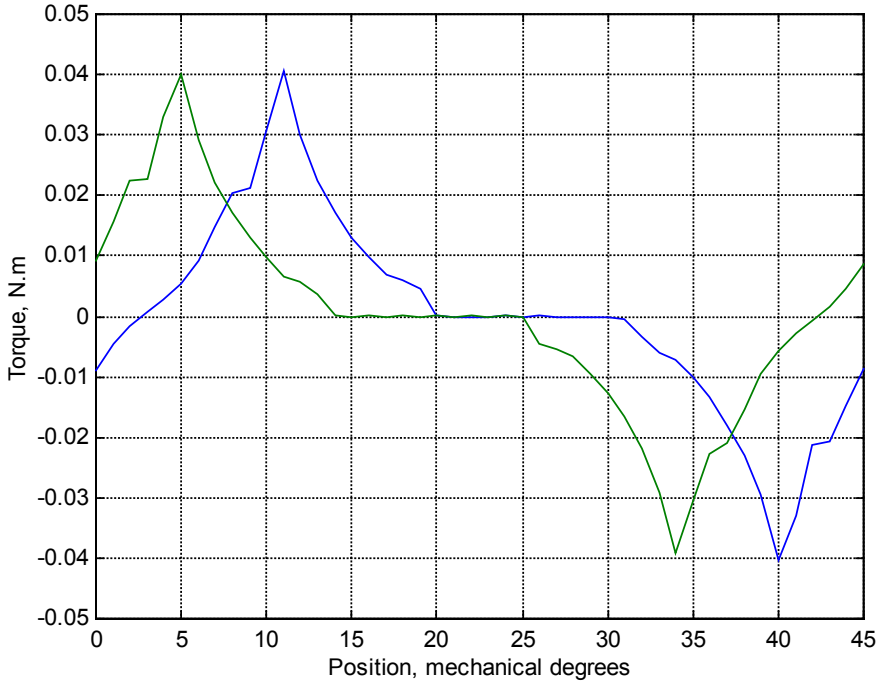

Figure 2.7 – Torque – Interpole pairs #1 and #2 energized

The prototype machine was constructed by Kartik Sitapati and is shown in figure 2.8 with all of its component parts in disassembled form. The minimization of component parts is obvious for this machine construction and that is an asset in applications.

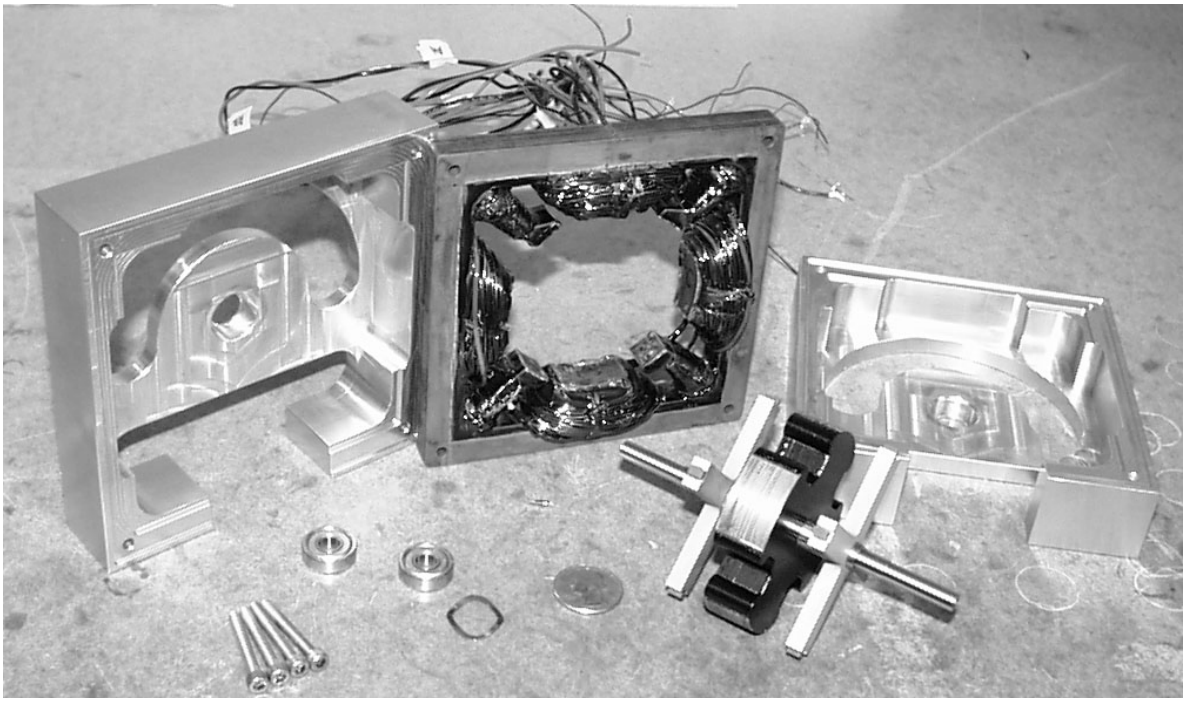

Figure 2.8 – Machine and components

2.2 Experimental Verification of Main Winding Inductance

2.2.1 Experimental Test Setup

In order to verify the main winding inductance, a separate circuit was utilized. A known resistance was placed in series with the main winding and a switch. A DC current at a specific level was applied to the resistance and winding and allowed to reach steady state. Then the switch was opened and the current in the winding was monitored for decay. From this decay rate, it was possible to determine the time constant of the RL circuit. From this time constant, the inductance could be calculated simply. The main winding resistance was taken into account since the main winding was not a pure inductor. The resistance of the winding was measured to be approximately 1.3 Ω. Each individual winding was measured to be approximately 0.3 Ω, which corresponds to the series connection total resistance of 1.3 Ω.

2.2.2 Experimental Results

The decay of the current is shown below in figure 2.9. The top curve (positive to negative going) represents the current sensed in the main winding using an oscilloscope current sensor. The bottom curve (negative to positive going) represents the feedback current, which is why it is negative. From the plot, it can be seen that the feedback is the exact same as the sensed current (except for the polarity). It is only necessary to determine the decay rate for one curve.

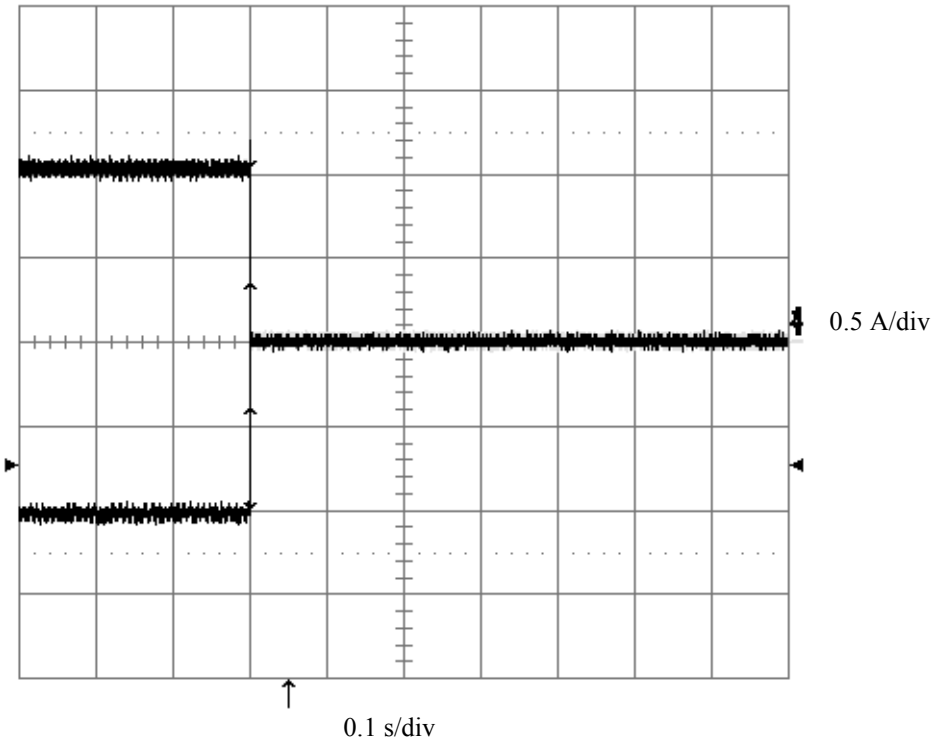

Figure 2.9 – Inductance Measurement at 1 A DC

Figure 2.10 shows the expanded view the decay of the current. From this plot, the amplitude of the current was measured and then the 63.2 % value of the current was determined and found on the curve. This point was then shifted to the axis for a marker, and then time cursors were used to determine the time between the point where the current first started to decay to the point when it reached the 63.2 % value. This value of time is equal to the time constant of the RL circuit. Table 2.1 shows the time constants and inductances for DC currents ranging from one Ampere to eight Amperes.

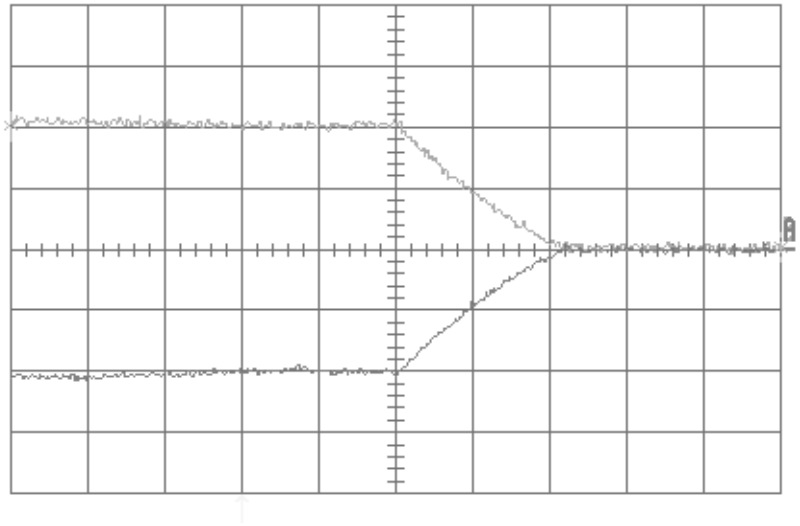

Figure 2.10 – Expanded Inductance Measurement at 1 A DC

I (A)	$I_{measure}$ (A)	63.2 % of $I_{measure}$	$\tau = \frac{L}{R}$	$R_{external}$ (Ω)	R_{total} (Ω)	L (mH)
1	1.01	0.6383	1.2290 ms	12.2	13.5	16.59150
2	1.98	1.2514	1.2547 ms	12.3	13.6	17.06392
3	2.96	1.8707	1.2538 ms	12.2	13.5	16.92630
4	3.83	2.4206	1.1642 ms	12.4	13.7	15.94954
5	5.06	3.1979	971.0 µs	11.9	13.2	12.81720
6	5.97	3.7730	796.4 µs	12.3	13.6	10.83104
7	6.75	4.2660	659.6 µs	11.9	13.2	8.70672
8	8.00	5.0565	533.4 µs	12.6	13.9	7.41426

Table 2.1 – Aligned Position Inductances for specific DC currents

Also, a measurement was taken for an unaligned inductance value. A small current of 0.25 A was passed through the setup while the rotor shaft was held at the unaligned position of 45 degrees. The same procedure as the one described in Section 2.2.1 was followed. The measure point was 0.22 A, and the 63.2 % point was 0.13904 A. This corresponded to a time constant of 220.1 µs. The external resistance was 12.1 Ω, and the total resistance was 13.4 Ω. The inductance value calculated was 2.95 mH.

In figure 2.11 the analytical results for an inductance profile at eight Amperes DC is given. Figure 2.12 presents the measured results for inductance profiles at currents ranging from one Ampere to eight Amperes DC. Actual measurement points are denoted on figure 2.12 with a dot. It can be seen that the measured results for eight Amperes does correspond to the analytical results for eight Amperes with some slight error. The peak inductance for the analytical results is approximately 5.55 mH while the experimental value is approximately 7.41 mH. The unaligned position analytical result is approximately 1.65 mH, while the experimental result is approximately 2.95 mH. The error is high, but it is still acceptable. From the shape of the inductance profile from the analytical analysis and the measured inductance points for aligned and unaligned positions, it was possible to extract the other inductance curves at different currents. As the current is decreased, the inductance rises. Also, it can be noted that the unaligned inductance does not vary much with decreasing current.

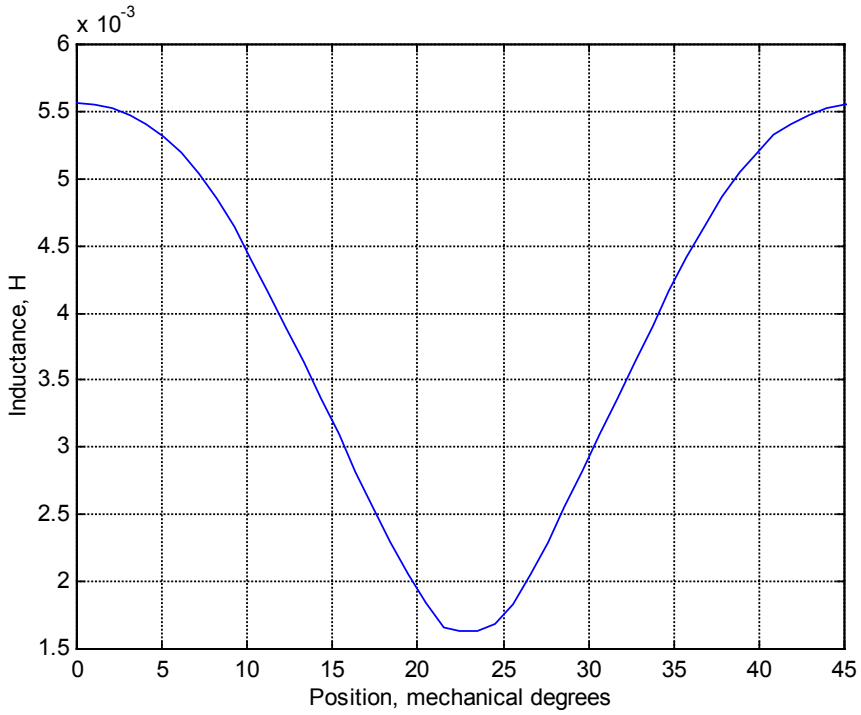

Figure 2.11 – Inductance Profile for 8 A DC From FEA Results

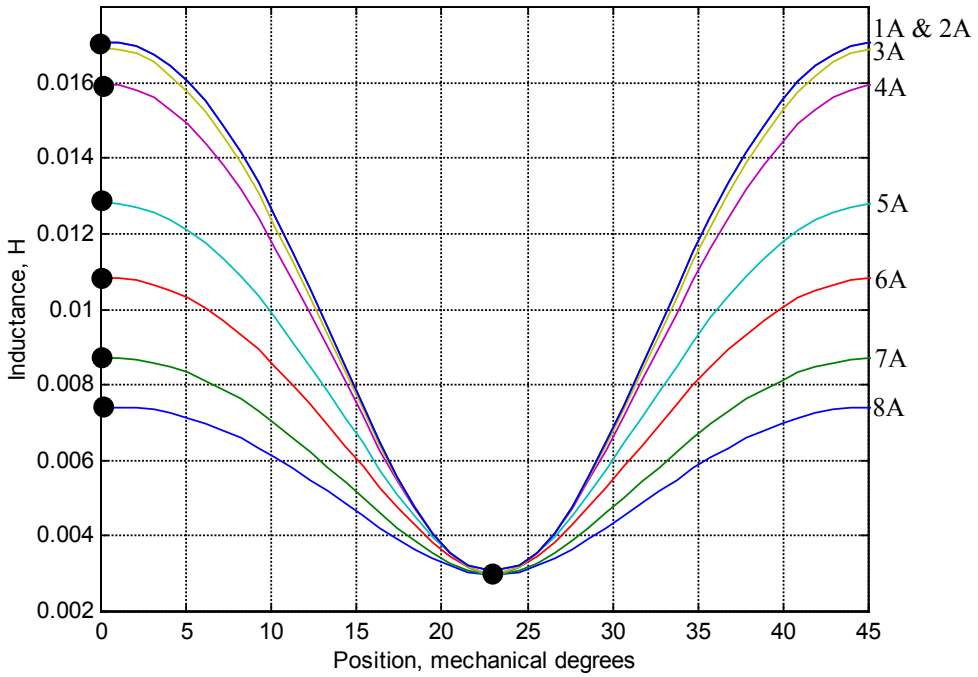

Figure 2.12 – Inductance Profiles for Specific DC Currents from Experimental Results and Interpolation

Chapter 3. Converter Selection

3.1 Purpose and Place in Drive System

The converter is a required element of a motor drive system. It is responsible for supplying the motor with power as well as commutation pulses to allow for rotation. The commutation pulses come from the semiconductor transistor switch. It has been shown in previous work [10] that it is possible to have only a single switch per phase, which is an important issue to low cost development of drive systems and one reason why single-phase systems appear popular. The firing sequence of the semiconductor transistor switch is developed in the control system not in the converter.

3.2 Alternatives

The most widely accepted converter for a single-phase SRM is the asymmetric bridge design. The asymmetric bridge begins with an ac supply fed into a bridge rectifier connected to

a DC link. This is then fed to the bridge, which consists of two transistor switches and two diodes. The windings are connected in between the first transistor and the cathode of the first diode and between the anode of the second diode and the second transistor. This design involves four semiconductor devices for each phase, two IGBTs and two power diodes.

Other configurations, such as the split supply converter and the C-dump converter, also require many semiconductor devices. The finalized converter design utilized only a single IGBT and a single power diode, which is why the converter presented is much more attractive than other options more commonly accepted.

3.3 Final Selection

3.3.1 Description

The converter used in this thesis was designed by Dr. Krishnan Ramu. It is shown in figure 3.1 and begins as a normal converter with a supply fed into a bridge rectifier with a DC link filter. This is where the similarities end. There is a branch, which acts as a voltage divider with filter to smooth a voltage of 12 volts clipped by a zener diode to power the necessary control circuitry, this is the section labeled as Logic Power Supply. Also, the converter has a built in current sensing resistor network, which relates current after the switch and after the snubber to the current in the main. So, when the switch is on, there will be current after the switch in RS1, and when the switch is off (during the on time of the main current), the current will flow through the snubber capacitor and through RS2. The addition of the currents sensed in these two resistors will give a total picture of the current in the main windings at any given time. Finally, there is a snubber circuit and an auxiliary winding circuit. The snubber is charged when there is current in the main windings, and when the current is zero, the snubber supplies the energy it stored to the auxiliaries. The auxiliary circuit requires an external resistor (significantly large power resistor) to limit the current in the auxiliary winding to less than two Amperes for which it is rated.

The significant factors influencing the converter design are the number of switching devices that determines heat sink volume and area and the number of logic power supplies. To

have a cost-efficient design it is imperative to have as few switching devices as possible. The proposed design uses a single switch for excitation of the main winding as well as for one interpole winding. For the time being, the second interpole is neglected and not used in the present study. A turn-off snubber is added to limit stress on the switch and also to provide the energy to one interpole winding. In that process, the energy obtained through the current control of main winding is effectively used to determine the level of excitation of the interpole winding. But, since the auxiliary windings will be continuously supplied, an external power resistor is preferable to limit the current.

In order to extend this system to sensorless applications, two small current sensing resistors have been added at the switch and after the snubber. By detecting the current through these two resistors, and the voltage across the snubber capacitor by means of another resistor divider combination, it is possible to estimate the rotor position, thereby eliminating the need for position sensors for control circuitry.

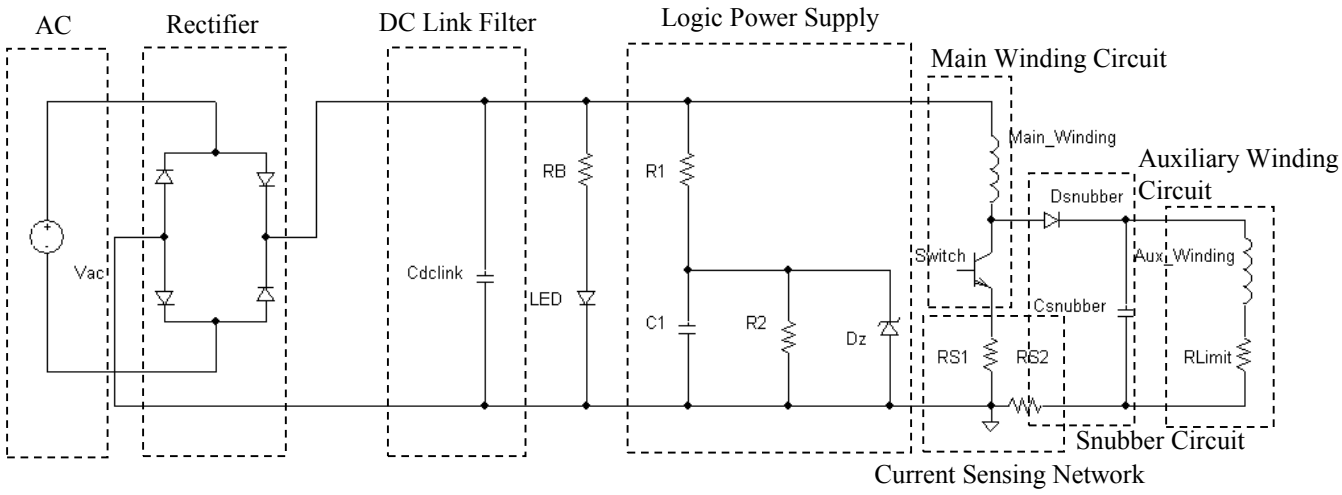

Figure 3.1 – Converter Design

3.3.2 Design Analysis

Up to this point, the work presented has been the work of others. Starting here, the work presented is contributed directly by the author of this thesis.

3.3.2.1 AC to DC Conversion

The first section of the converter involves an AC to DC conversion. An AC to DC converter is necessary to power the drive and derive power sources for other circuitry necessary. Most projects would simply opt to use a prepackaged converter, but this research was concentrated on minimum component, minimal cost design; therefore, the AC to DC conversion section was also pieced together and built. A full wave bridge rectifier with a DC Link Filter was chosen for the design. Its specifications are laid out below.

The first step to determining the components of the converter was to determine the duty cycle. First, the inductance profile was approximated and the shape of the winding current waveform was fitted to it to determine the appropriate switching point.

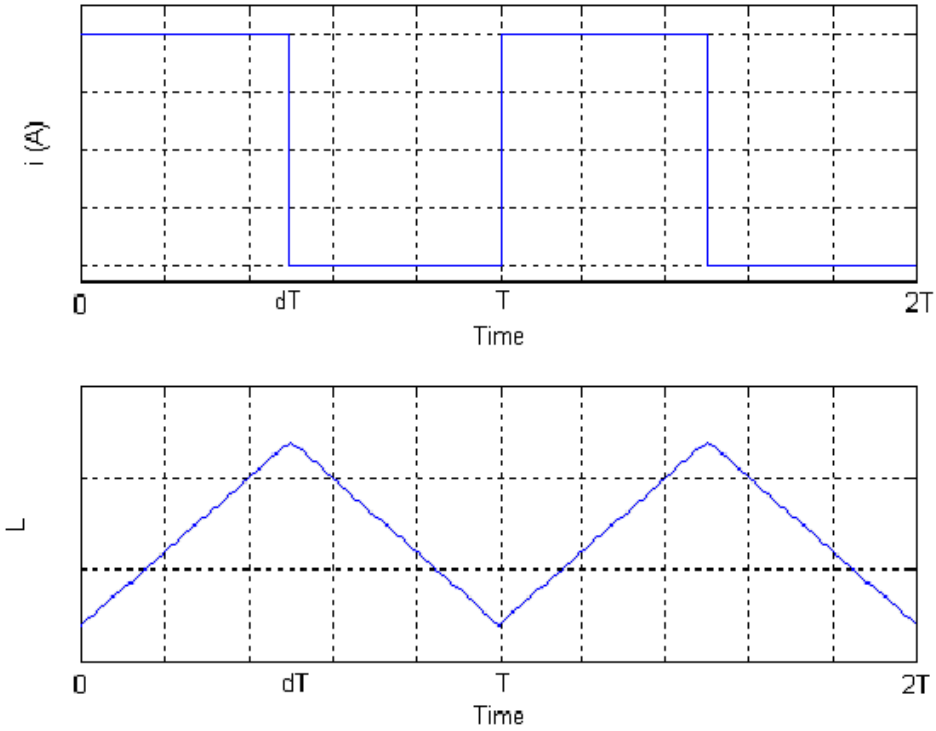

Figure 3.2 – Typical Inductance and Main Current Profiles

In order to switch at the point of maximum inductance, dT must equal ½T, this lead to a duty cycle of ½.

Next, the amount of average current required must be determined in order to accurately size the bridge rectifier for the AC to DC converter section.

$$I_a = \frac{1}{T}\int_0^{dT} i\,dt = \frac{1}{T}\int_0^{dT} 8\,dt = \frac{1}{T}\left[8t\right]_0^{dT} = \frac{8dT}{T} = 8d = 8\left(\frac{1}{2}\right) = \underline{\underline{4A}}$$

From the current specification above, the bridge rectifier had to be able to provide 4 Amperes average current. They also had to be able to handle a reverse voltage equal to V_{DC}.

$$V_{D1} = V_{DC} = \left(\sqrt{2}\right)V_S = \left(\sqrt{2}\right)(120V) = 169.71 Volts$$
$$For\ safety:\ Spec = 1.5V_{D1} = 1.5(169.1 Volts) = 254.56\ Volts$$

The Diode rating for the Full Bridge Rectifier circuit was {400 Volts, 4 Amps}.

In order to complete the AC to DC conversion section, the DC Link capacitor had to be accurately sized. Also, this capacitor had to be able to withstand more of a voltage than was required for normal operation for safety. An aluminum electric capacitor with a 250 Volt rating was used. The sizing analysis follows:

$$Energy\ supplied\ to\ the\ circuit\ in\ one\ cycle = V_{DC} i_a t = \frac{1}{2} C_{DCLink} V_{DC}^2$$
$$t = dT\ which\ relates\ to\ t_{on}\ time\ when\ current\ is\ flowing$$
$$C_{DCLink} = \frac{2i_a dT}{V_{DC}} = \frac{8T}{\sqrt{2}(120)} = 0.04714T$$
$$T = time\ to\ complete\ \frac{1}{4}\ of\ a\ revolution \Rightarrow assume\ a\ base\ speed\ of\ 1500\ rpm$$
$$0.25\ rev = 1500\frac{rev}{\min}(T) \Rightarrow T = 0.00016666 \min\left(\frac{60\ \sec}{1\ \min}\right) = 10\ ms$$
$$C_{DCLink} = 0.04714(0.010) = 471.4\ \mu F \Rightarrow \underline{\underline{1000\mu F,\ 250\ V}}$$

For safety's sake, a bleed resistor and a LED were put in parallel with the DC Link capacitor. Concerns for the sizing of this bleed-off resistor included the power that it must be able to withstand and the time constant that it forms with the DC Link capacitor. This time constant must be small in order to drain all of the charge from the capacitor quickly. The LED was neglected in the sizing analysis, since the voltage that it operates at is very low. The LED's

only purpose was to be a physical signal to indicate when the capacitor was still draining through the resistor.

$$P = \frac{V_{DC}{}^2}{R_B} = 1\ Watt = \frac{(169.71\ Volts)^2}{R_B} \Rightarrow R_B = 28.8\ k\Omega \Rightarrow \underline{\underline{R_B = 40\ k\Omega, 1\ W}}$$
$$\tau = R_B C_{DCLink} = (40\ k\Omega)(470\mu F) = 18.8\ s$$

This time constant was on the large side, but it was necessary to keep the size of the resistor to a minimum. Most resistors with a power rating of higher than one Watt are large in size and can be costly.

3.3.2.2 Control Circuit Power Supply

The next phase for this converter was the power supply branch for the control circuitry. In order to avoid having to add a separate power supply for the controls, which typically run on 5 to 20 Volt supplies, a supply was been built into the converter topology to provide for a single 12 Volt supply to power all circuitry necessary from sensors to operational amplifiers. This circuit design required the utmost of consideration in order to draw enough current into the branch but still be close to the required 12 Volts in order to allow for appropriate regulation by the zener diode.

In order to adequately power the control circuit, 100 mA would be an optimal amount of current to be drawn into the branch. A great deal of this current would be lost within the voltage divider circuit and the rest would be used to power the zener as well as the attached controls. First, the top resistor of the voltage divider was to be determined:

$$V_{DC} - 12 Volts = I_{R_1} R_1$$
$$R_1 = \frac{V_{DC} - 12}{I_{R_1}} = \frac{169.71\ Volts - 12}{100\,mA} = 1.57\,k\Omega$$
$$P = \frac{(V_{DC} - 12)^2}{R_1} = \frac{(157.71\ V)^2}{1.57\ k\Omega} = 15\ Watts$$

This value would allow for the right amount of current, but a 15-Watt resistor would be too large, and too much energy would be expended in this resistor.

$$P = \frac{(V_{DC} - 12)^2}{R_1} = 7\ W = \frac{(157.71\ V)^2}{R_1} \Rightarrow R_1 = 3553\ \Omega \Rightarrow \underline{\underline{R_1 = 4\ k\Omega,\ 7\ W}}$$

$$V_{DC} - 12 Volts = I_{R_1} R_1$$

$$I_{R_1} = \frac{V_{DC} - 12}{R_1} = \frac{169.71\ Volts - 12}{4\ k\Omega} = 39.4\ mA$$

The 39.4 mA was not quite the desired amount of current, but it was sufficient.

From here, it was possible to determine the second resistor of the voltage divider in order to provide 12 Volts at the zener. This voltage had to be close to that of the desired regulated voltage by the zener. Since, it was known that R_1 must be a 4 kΩ, the straightforward equations of a voltage divider were used to determine R_2.

$$12\ Volts = V_{DC}\left(\frac{R_2}{R_1 + R_2}\right) = 169.71\left(\frac{R_2}{4\ k\Omega + R_2}\right)$$

$$48{,}000 + 12R_2 = 169.71R_2 \Rightarrow 157.71R_2 = 48{,}000$$

$$R_2 = 324.96\ \Omega$$

$$P = \frac{(12\ V)^2}{R_2} = \frac{(12\ V)^2}{324.96} = 0.44\ W$$

$$\underline{\underline{R_2 = 100\ \Omega,\ \frac{1}{2}\ W\ and\ a\ 500\ \Omega\ Potentiometer}}$$

A known resistor in series with a potentiometer that can be adjusted to get an exact 12 Volts was used for R_2.

The capacitor in the control power supply branch had two significant purposes. First, it smoothed and filtered the voltage that was used to supply the control circuitry. Second, its discharge was used to continuously supply voltage to the circuitry to ensure a supply.

The zener diode had to be able to regulate the voltage to 12 Volts. It must also require a minimal amount of current. For these reasons, a 1N5242 Zener Diode with 12 Volt, ½ Watt characteristics was chosen. It held the voltage right at 12 Volts and required only 8 mA of current to function properly.

3.3.2.3 Current Sensing Scheme

In place of using expensive, bulky current sensors, current sensing resistors were used. They were placed in strategic locations in order to monitor the current in the main windings. With the addition of the current at the emitter of the IGBT and at the base of the auxiliary windings and snubbering circuit, it was possible to monitor the current in the main winding at all times. These were not designed per se, except to note that they must be small in order to not create a voltage drop. They were set as small as possible. 0.01-Ohm sensing resistors were used.

3.3.2.3 Semiconductor Switch

At the heart of this converter is the semiconductor switch that is used to allow for controllable firing. An IGBT was chosen for the controllable switch in this converter. This device needed to be able to handle current of at least eight Amperes peak and 340 Volts. In case of current spikes, it must be able to handle much more than eight Amperes. An International Rectifier G4PC40U IGBT was selected. This device is rated for 40 Amperes and 400 Volts.

3.3.2.5 Snubbering Circuit

The snubbering circuit had many purposes. First, it was employed to reduce stress on the IGBT, and second, its energy was used to supply the auxiliary winding circuit. It was required in order fully utilize the interpoles and still retain a single-switch design.

The design of the snubber capacitor was one of the most critical. If it was too large then it would store too much energy and would not allow the main winding current to go to zero when the switching stops. But, if it is too small, then the auxiliary windings would not be supplied with enough energy to be of any use. The size must allow the energy in the capacitor to be equal to the energy in the main winding.

$$\frac{1}{2}C_{snubber}\left(V_{snubber}\right)^2 = \frac{1}{2}L_{main}\left(I_{main}\right)^2$$

In order to determine the size of the capacitor, data was taken for the voltage that it would store. At first, a 100 μF, 450 V aluminum electric capacitor was used in all the initial

calculation, and it was found to be too large. Also, with a full reference command given, the maximum attainable speed was noted. The data taken follows below in table 3.1.

V_{ac} (V)	V_{dc} (V)	$V_{snubber}$ (V)	Maximum Speed (RPM)
10.00	10.0	16.0	1920
20.53	23.9	36.5	3218
30.33	34.9	57.0	4160
40.5	49.0	73.0	5140
50.3	61.5	94.2	6080
60.2	74.0	145.0	6295
70	91.5	197.0	7145
80	104.0	220.0	7855
90	115.5	242.0	8545
100	126.0	268.0	9000
110	131.0	288.0	9061

Table 3.1 – Snubber Capacitor Calculation Required Experimental Values

From the values above and using a worst-case analysis, it was possible to determine the precise value that the capacitor should be. From the inductance measurements in Section 2.2.2, the inductance for a peak current of eight Amperes or an average current of 4.0 Amperes was approximately 7.414 mH.

$$\frac{1}{2}C_{snubber}\left(V_{snubber}\right)^2 = \frac{1}{2}L_{main}\left(I_{main}\right)^2$$

$$C_{snubber} = \frac{L_{main}\left(I_{main}\right)^2}{\left(V_{snubber}\right)^2}$$

$$C_{snubber} = \frac{7.414\ mH\left(4\ A\right)^2}{\left(339.42\right)^2} = 1.03\ \mu F$$

$$\underline{\underline{C_{snubber} = 4.7\ \mu F,\ 450\ V}}$$

A snubbering capacitor of 4.7 microfarads was used instead of a one microfarad capacitor in order to allow for enough energy to be stored and transferred. A one microfarad capacitor was

right on the borderline of being able to store enough energy. A 4.7 microfarad capacitor was not large enough to seriously inhibit the fall of current in the main windings during the off time, but it was large enough to store enough energy to allow for current in the auxiliary windings during the off period.

Since the snubber capacitor voltage was at its highest at 339.42 Volts, the auxiliary circuit power diode had to be able to withstand at least that, and it was better if it could withstand more for safety. The power diode chosen was a 40EPF04, which has a current rating of 40 Amperes and a voltage rating of 400 Volts.

3.3.2.6 External Resistor for Auxiliary Winding Current Limiting

The final component of the converter circuitry was a resistor combined in series with the auxiliary windings. This resistor was necessary in order to limit the current in the auxiliary since the windings were only designed for a maximum of two Amperes. This resistor was a large external resistor. In future designs, it would be best to design another way to limit the current in the auxiliary in order to reduce cost, size, and loss that this resistor contributes.

$$2V_{DC} = I_{AUX} R_{LIMIT}$$

$$2(169.71\ V) = (2\ A)(R_{LIMIT}) \Rightarrow R_{LIMIT} \geq 169.71\ \Omega$$

Neglect auxiliary winding resistance since it is small.

225 W is the largest Power Resistor resonably available. Design for a power of 200 Watts.

$$P = \frac{(2V_{DC})^2}{R_{LIMIT}} = 200\ W$$

$$R_{LIMIT} = \frac{(339.42\ V)^2}{200\ W} = 576\ \Omega \qquad Try\ R_{LIMIT} = 1000\ \Omega$$

$$I_{AUX} = \frac{2V_{DC}}{R_{LIMIT}} = \frac{339.42\ V}{1000\ \Omega} = 0.33942\ A \quad This\ is\ sufficient\ to\ pull.$$

$$\underline{\underline{R_{LIMIT} = 1000\ \Omega,\ 225\ W - Wirewound\ Lug\ Power\ Resistor}}$$

3.3.3 Advantages and Disadvantages

There are many advantages as well as some disadvantages to using this circuit. The advantages include:

(i) Permanent magnets and other distinct mechanical means are not necessary for starting with the interpole design.

(ii) Design is compact and services both windings.

(iii) Only one controllable switch and one diode is required for all of the windings allowing for the lowest cost possible.

(iv) Capability as good as one-switch based DC drives and for the first time a true competitor to a single switch based chopper fed brush dc drive is made possible with this innovation of power circuit.

(v) Control circuit isolation is not necessary since the switch gate signal is with respect to the common.

(vi) Only common for current sensing and estimating position

(vii) Auxiliary winding is excited by the snubbing energy thus serving two needs.

(viii) Rotor position sensing is continuous since the auxiliary winding current is continuous.

(ix) Sensors are not required for sensorless operation since sensing resistors and interpoles are involved in the design of the system thus providing an inexpensive solution to a critical aspect of the single-phase SRM drive system.

The disadvantages include:

(i) The interpole winding continuously produces torque, which may generate some noise, but the net torque that is produced by the interpole winding is zero. If the interpole torque has to be utilized for load application, then it requires its own controlled switching power device.

(iii) There is a need for an external resistor in order to limit the current through the auxiliary winding, which contributes to energy losses and adds to the size of the system.

Chapter 4. Control Design

4.1 Design Approach

The objective of this section is to test the concept of the novel machine and converter. Accordingly, the sensorless operation was not considered. Also, only a simple control algorithm and strategy was devised for the basic testing of the prototype single-phase SRM drive system. The control system is shown in figure 4.1. Hall effect sensors were used to ascertain the rotor position and speed. The sensor output was then converted to a speed reference, which was subtracted from a speed command to give an error to feed the control logic. First, a proportional plus integral (PI) controller converted the error into the current command, which was limited and sent to the current control loop. Control voltage was obtained from the current error that was the difference between the current command and feedback current. The current error was amplified through a proportional plus integral controller to yield the final control voltage. This control voltage was then sent to a PWM chip. The PWM IC generated a 20 kHz square output, which was compared with the control voltage to give a certain duty cycle with a square wave output. This output signal with a variable duty cycle was logically anded with the hall sensor output to produce a gate drive signal for the IGBT switch.

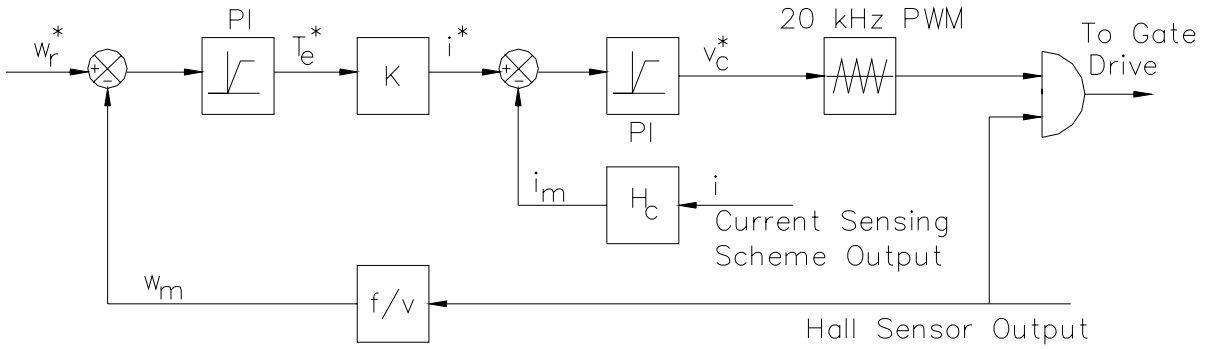

Figure 4.1 – Control Methodology Block Diagram

4.2 Components Design

In experimental practice, each stage of the control was designed and then implemented. Each phase was experimentally verified before moving on to the next part. The signal at the gate was designed first, and then control loops were built around each previous section. The design will be presented here in the same fashion.

4.2.1 PWM Control and Gate Drive Signal

The first part of the control deals with delivering a signal to the gate of the semiconductor switch in order to have accurate and precise firing of the phase to allow for proper rotation. This gate drive signal was dependent on the output of the hall sensors and the output of the PWM. First, we will explore the hall sensor outputs.

Two hall sensors were fastened to the endbell of the machine in fixtures that were manufactured to have the same curvature as the endbell opening. These fixtures were also at a particular height that allows magnets that are connected to a fixture on the rotor and shaft to have minimal clearance over the sensors when the machine is in motion. These sensors were attached at the zero degree (maximum inductance) and 45 degree (minimum inductance) points to indicate turn on and turn off pulses, which is shown in figure 4.2. The sensors used were bipolar Hall effect latches that change from zero to V_{cc} with a change in the magnetic field. They latch at a particular level until a new pole passes over them.

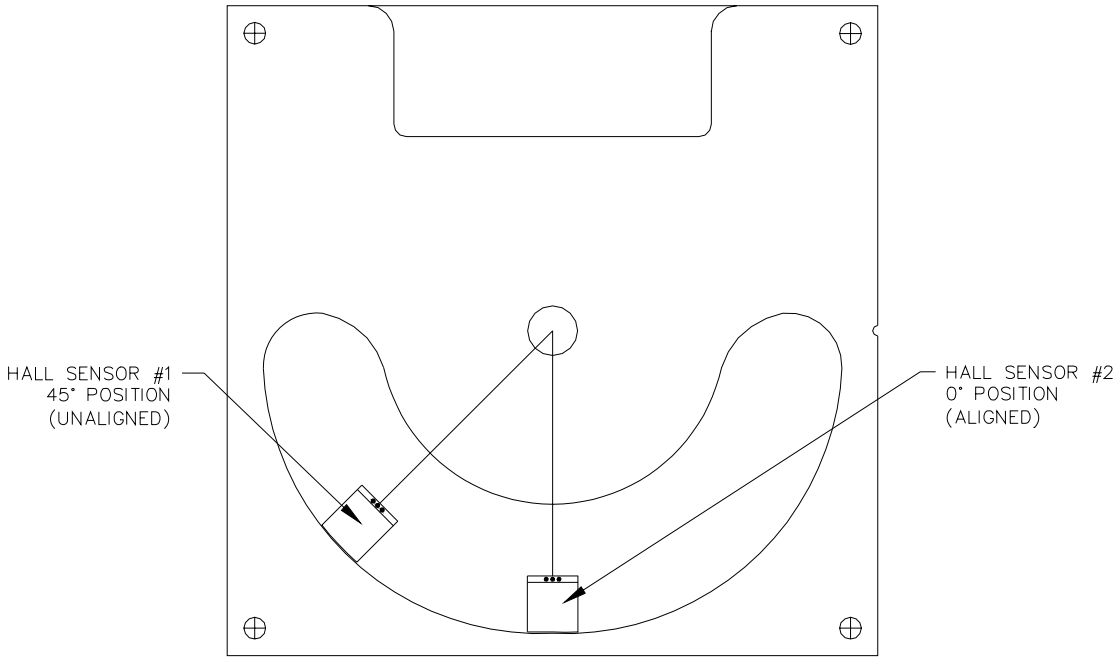

Figure 4.2 – Hall Sensor Attachments to the Endbell

When the sensor signals were both low it was required the gate signal to be low as well. If either one was high, then the position gate signal was also required to be high. If both signals were high, it was required the position gate signal to be low. This was basically an Exclusive-OR connection. This is shown in the graph and truth table below.

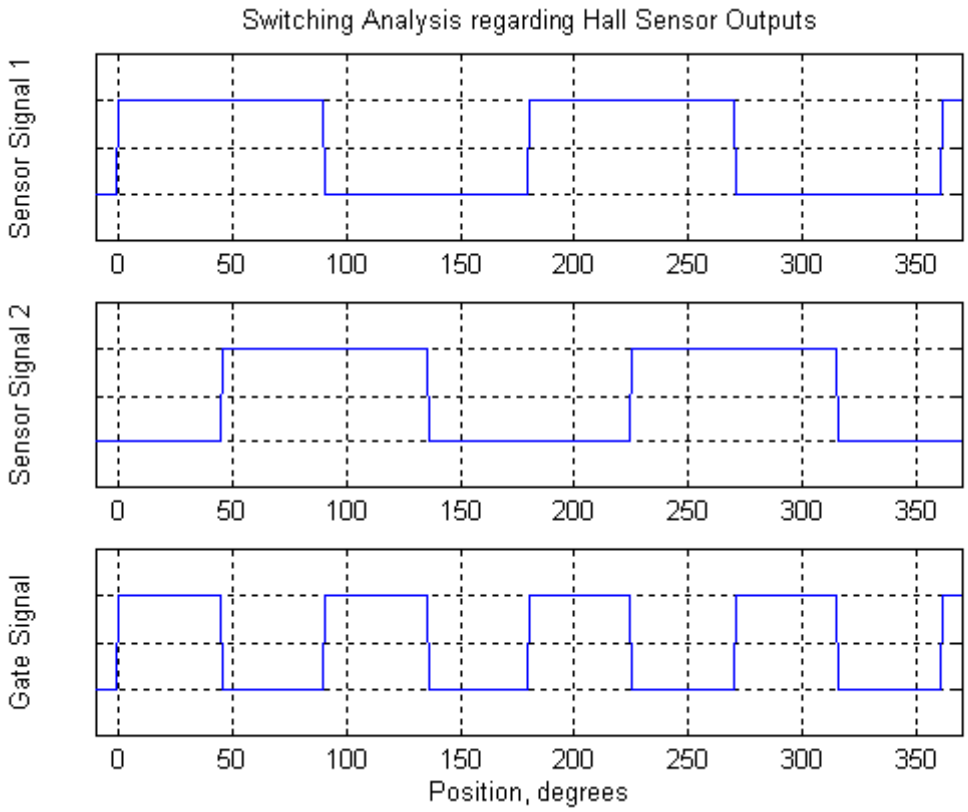

Figure 4.3 – Switching Analysis regarding Hall Sensor Outputs

Sensor Signal 1	Sensor Signal 2	Position Gate Signal
0	0	0
0	1	1
1	0	1
1	1	0

Table 4.1 – Truth Table for Sensor Signals to Gate Signal Output

A Texas Instruments CD4030BE (CMOS Quad Exclusive-OR Gate) was used to provide this output given the input of the sensor signals. The connections from the sensors to this chip are shown in figure 4.4. It can be seen from the graph above, four complete switching cycles are required for each complete revolution.

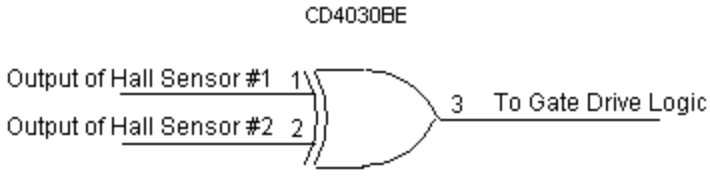

Figure 4.4 – Hall Sensor to Exclusive Or Logical Connections

The gate drive signal was also dependent on the output of a PWM IC. All of the connections for this IC are shown in figure 4.5. The PWM chip that was used in this research was a Texas Instruments UC3524 (Advanced Regulating Pulse Width Modulator). This chip is a single frequency pulse width modulation voltage regulator control circuit. A single timing resistor and a single timing capacitor determine the frequency of operation. The equation to determine the values of these components is given in the data sheet, and the calculations required follow below.

$$f = \frac{1.18}{R_T C_T}$$

$$Set\ C_T = 0.01\ \mu F\ \ for\ convenience\ and\ set\ f = 20\ kHz$$

$$20\ kHz = \frac{1.18}{R_T(0.01\ \mu F)}$$

$$R_T = 5.9\ k\Omega$$

$$\underline{\underline{R_T = 5.6\ k\Omega\ in\ series\ with\ a\ 500\ \Omega\ potentiometer}}$$

A 5.6 kΩ resistor was used in series with a 500 Ω potentiometer to adjust the oscillation to have a period of exactly 50 μs. The timing capacitor generates a ramp function of the designed frequency, and then it is compared to the error between the inputs. This is then used to generate a pulse train with a specific duty cycle depending on the input level. This duty cycle to input signal ratio was verified experimentally. The table below demonstrates the proportions used.

Input Voltage in PWM Circuit	Resulting Duty Cycle
0.8 Volts	0 %
3.53 Volts	100 %

Table 4.2 – PWM Input Voltage and the Resulting Duty Cycle in the Output

In order to power the IC, pins eight, 15, and 16 are used. Pin 15 is the power pin and pin eight is the ground pin. Pin 16 is only used when a five volt reference supply is necessary for the circuitry, but in this research the internal regulator was sufficient. Pin 16 was grounded through a 0.1 microfarad capacitor as recommended in the datasheet.

This chip also has the capability to be a protection device, since it has current limiting ability and shutdown ability. These functions were not utilized in this design; therefore, pins four and five were grounded for the current limiting, and pin 10 for shutdown was left floating as recommended in the datasheet.

The outputs of this IC are open collector outputs and can be tied together for single-ended applications. In this research, the collectors (pins 12 and 13) were tied together and pulled up to power through a resistor. The emitters were tied together and used as the output for the PWM which is used as an input for the gate drive logic circuit.

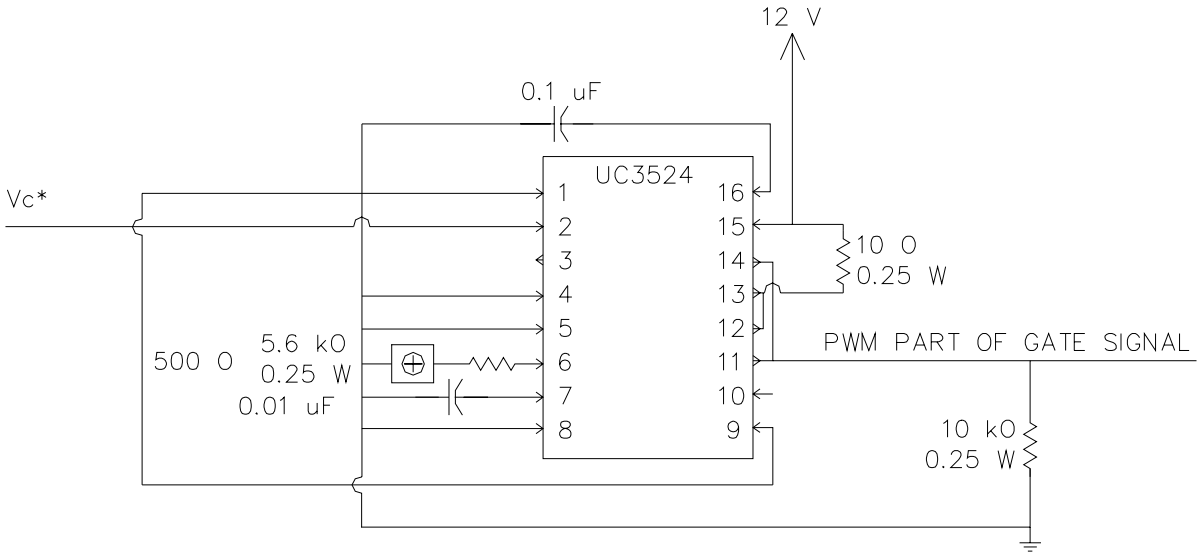

Figure 4.5 – PWM IC Connections

The gate drive signal was a combination of the Hall sensor outputs and the PWM IC output. It was desired to have the magnitude of the Hall sensor output with the switching of the PWM IC output. This was a logical AND connection. A Texas Instruments CD4081BE (CMOS Quad 2-input AND gate) was used to generate the final gate signal. Its connections can be seen in figure 4.6. Pins one and two are the inputs to a two-input AND gate. Pin three is the output of the corresponding gate. Pin 14 is the power pin, and pin seven is the ground pin. This gate signal had the amplitude level of the position output from the hall sensor combination and it had the switching duty cycle of the PWM output. The desired gate signal can be seen in figure 4.7.

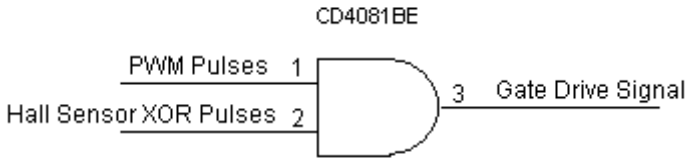

Figure 4.6 – Gate Drive Logic Circuit Connections

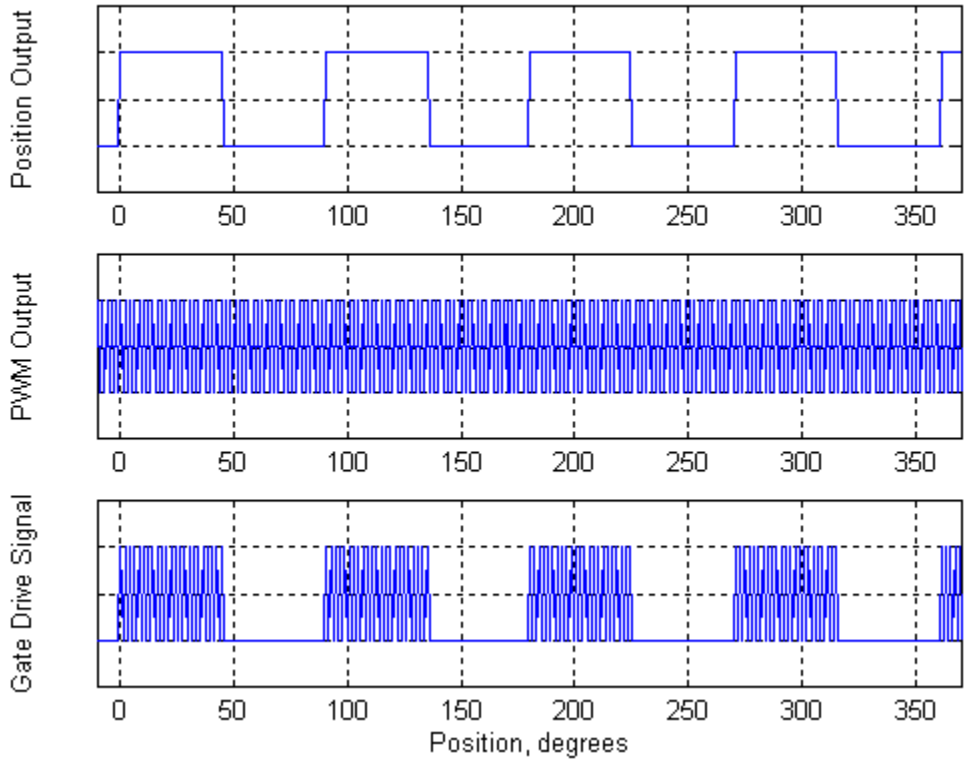

Figure 4.7 – Gate Drive Signal Generation Analysis

4.2.2 Current Control Loop

Once the form of the gate drive signal had been established, the signals needed were derived by working backwards. The only signal missing was the control voltage signal that was required by the PWM IC. This was the signal that was to be generated by the current control loop. The form of the current control loop is shown in figure 4.8. A dashed line is drawn around each segment and its section of discussion is noted. The entire current control loop logical schematic is shown in Appendix C. The actual wiring diagram for the current control loop is shown in Appendix D.

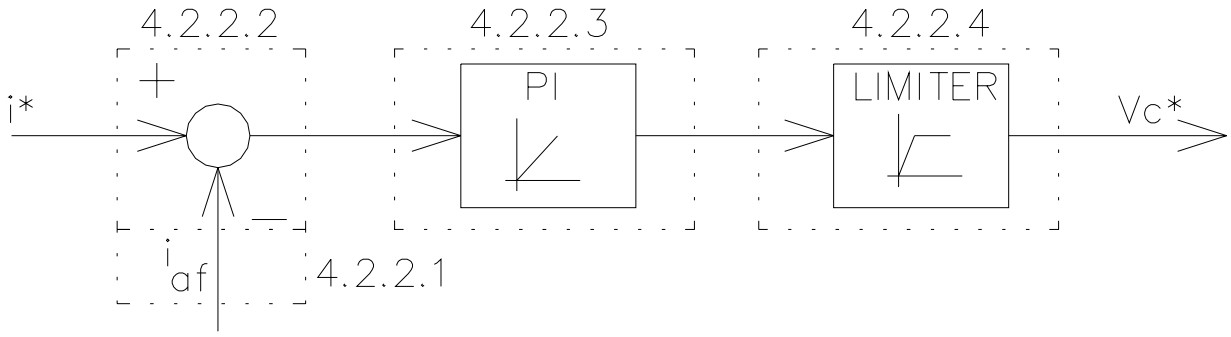

Figure 4.8 – Current Control Loop Block Diagram

4.2.2.1 Current Feedback

The first step in current control was to first be aware of the current that is in the system. Most systems utilize current sensors to have current feedback. These sensors can be bulky and expensive; therefore, we opted for inexpensive, small current sensing resistors. They were placed in strategic locations within the converter circuit. Since, they are such small resistances, they have no effect on the circuit and are negligible in calculations. With full current in the windings, there will be a maximum voltage drop of 0.08 Volts.

$$V = IR$$
$$V = (8\ A)(0.01\ \Omega) = 0.08\ V$$

At first, it was believed that only the resistor in series with the switch was required for the feedback, but it was found that when the machine was unloaded, there was a significant amount of current in the auxiliary windings. This current was not being taken into account as having been in the main winding, and accordingly, the feedback was not truly indicative of the current flowing in the main windings. In order to solve this problem, a summing amplifier was used to add the feedback from both resistors together before using it as the total feedback. In a future design, a single current resistor could be used in between the ground and the node, which connects the switch, snubber capacitor, and auxiliary windings. This configuration is seen below.

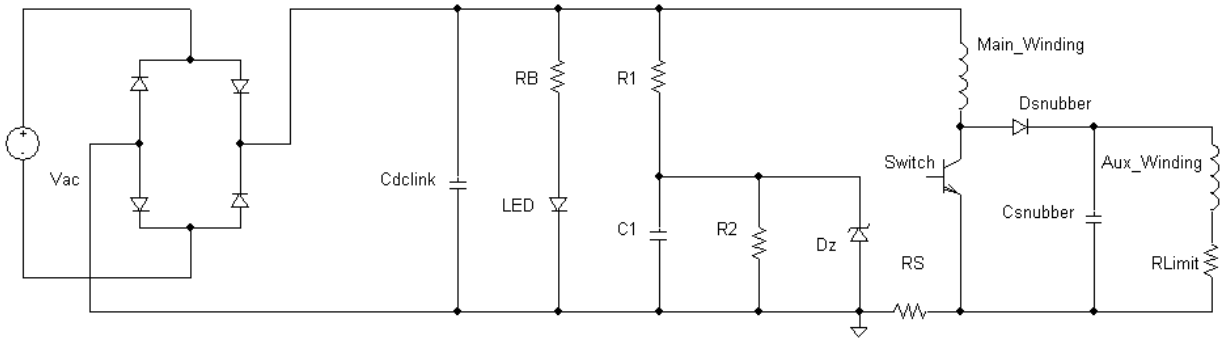

Figure 4.9 – Alternate Sensing Configuration Converter

For this research, the original converter design was used. A summing amplifier was constructed. LM324AN (Quad Operational Amplifiers) were used in the construction of all control circuitry. These chips were used because they require only a single positive supply of 12 Volts, which was perfectly suited to the supply circuit derived from the converter. But, there is a drawback to the use of this chip. The LM324AN IC requires the use of only noninverting amplifiers since they have no negative reference. Therefore, all stages were built in a noninverting configuration. The design of the summer follows below. Since all of the resistors are of the same value, the equations work out so the output in not dependent on their value; therefore, a standard value of 1 kΩ was chosen.

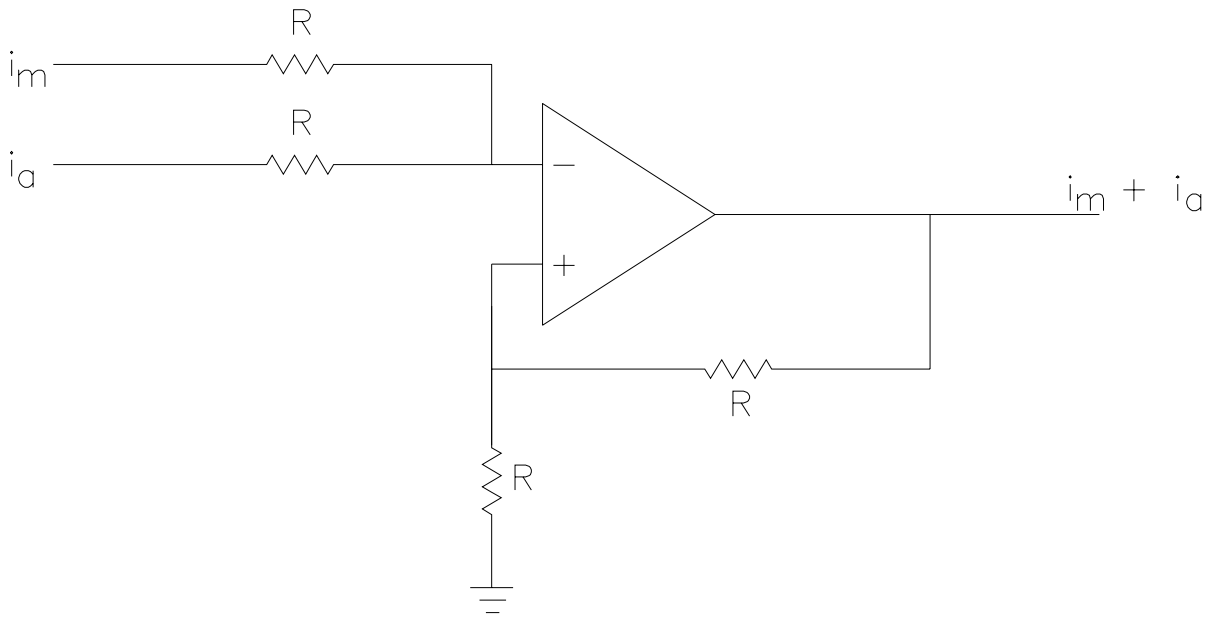

Figure 4.10 – Summing Amplifier for Current Feedback

Noninverting Terminal:

$$\frac{V - V_{RS1}}{R} + \frac{V - V_{RS2}}{R} = 0$$

$$V\left(\frac{2}{R}\right) = \frac{V_{RS1} + V_{RS2}}{R}$$

$$V = \frac{V_{RS1} + V_{RS2}}{2}$$

Inverting Terminal:

$$\frac{V - 0}{R} + \frac{V - V_O}{R} = 0$$

$$V\left(\frac{2}{R}\right) = \frac{V_O}{R}$$

$$V_O = 2V = 2\left(\frac{V_{RS1} + V_{RS2}}{2}\right)$$

$$\underline{\underline{V_O = V_{RS1} + V_{RS2}}}$$

Next, a gain determination was made. The maximum output voltage from the summer was 0.08 Volts, which represents a full current situation. The reference was evaluated at this point. Knowing that the output of the speed control loop (current command) would be limited, it was decided that the current command would be limited to a maximum voltage of 4.7 Volts. Therefore, the full current condition of 0.08 Volts must equate to the full current command of 4.7 Volts. If the command was all the way high, and the current in the winding was also full, there would be no error. The following equation was utilized:

$$\frac{4.7\ Volts}{0.08\ Volts} = A_V$$

$$\underline{\underline{A_V = 58.75}}$$

A simple noninverting gain amplifier was designed. The gain designed for was 60. A standard value of 1 kΩ was selected for R_1, and R_2 was solved for accordingly.

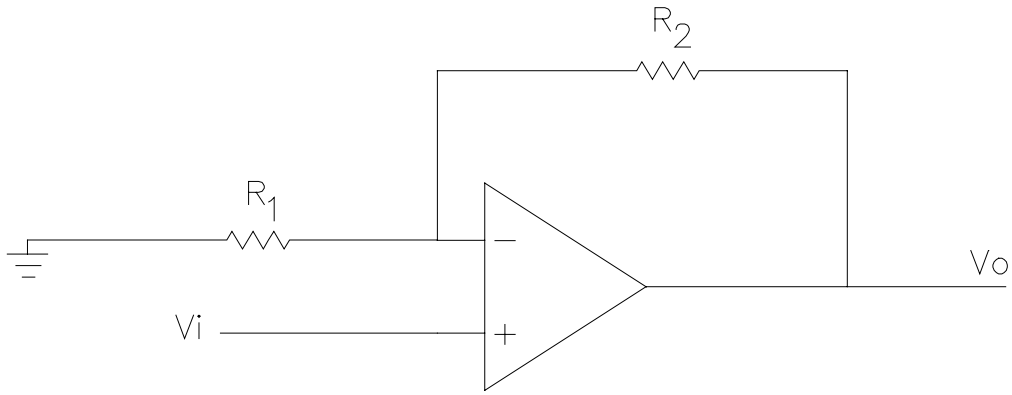

Figure 4.11 – Gain Amplifier for Current Feedback

Noninverting Terminal:

$$V = V_{O-Summer}$$

Inverting Terminal:

$$\frac{V-0}{R_1} + \frac{V-V_O}{R_2} = 0$$

$$V\left(\frac{1}{R_1} + \frac{1}{R_2}\right) = \frac{V_O}{R_2}$$

$$V_O = V_{O-Summer}\left(\frac{R_2}{R_1} + 1\right)$$

$$\frac{i_{amplified\ \ feedback}}{i_{feedback}} = A = \frac{R_2}{R_1} + 1$$

$$A = 60 = \frac{R_2}{1\ k\Omega} + 1 \qquad R_2 = 59\ k\Omega$$

$$\underline{\underline{R_1 = 1\ k\Omega \qquad R_2 = 59\ k\Omega}}$$

In order to ensure that the feedback was correct, the amplified signal was compared to the sensed current in the main windings using a current monitor attached to a scope. The resulting

waveforms are seen in figure 4.12. It can be seen from these waveforms that the shape of the current feedback does match that of the actual current in the windings.

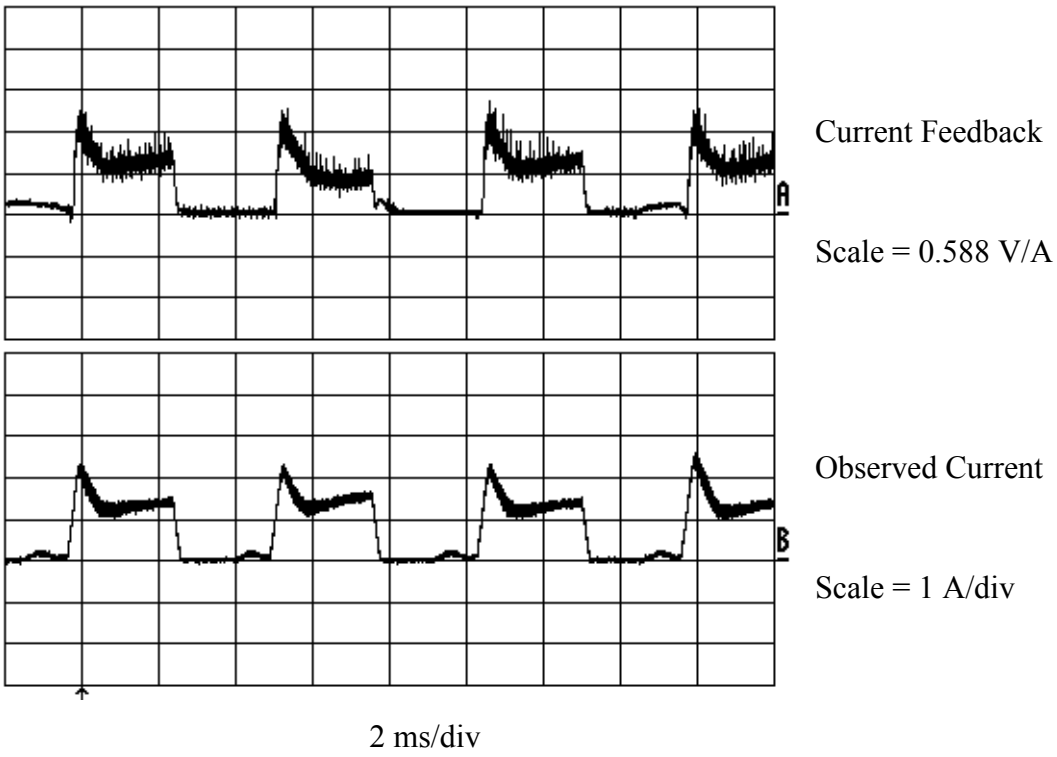

Figure 4.12 – Current Feedback and Current in the Main Winding

At this point, the feedback was ready to be compared to the reference to give an error and generate a control signal for the PWM IC.

4.2.2.2 Current Error Determination

In order to determine the error, the feedback had to be subtracted from the command. This was performed by way of a subtractor circuit with a gain of 1. The design justification is derived below. Since all of the resistors are of the same value, the equations work out so the output in not dependent on their value; therefore, a standard value of 1 kΩ was chosen. But, when this circuit was put into practice, an offset was discovered. This offset was the result of a voltage drop across the resistor fed by the current command. This voltage drop was being reflected onto the input pins of the operational amplifier and thereby onto the output. This led the output to show an error even if there was not one. In order to eliminate this problem, the

resistance used was increased to 100 kΩ. Once these resistors were changed, the offset was eliminated.

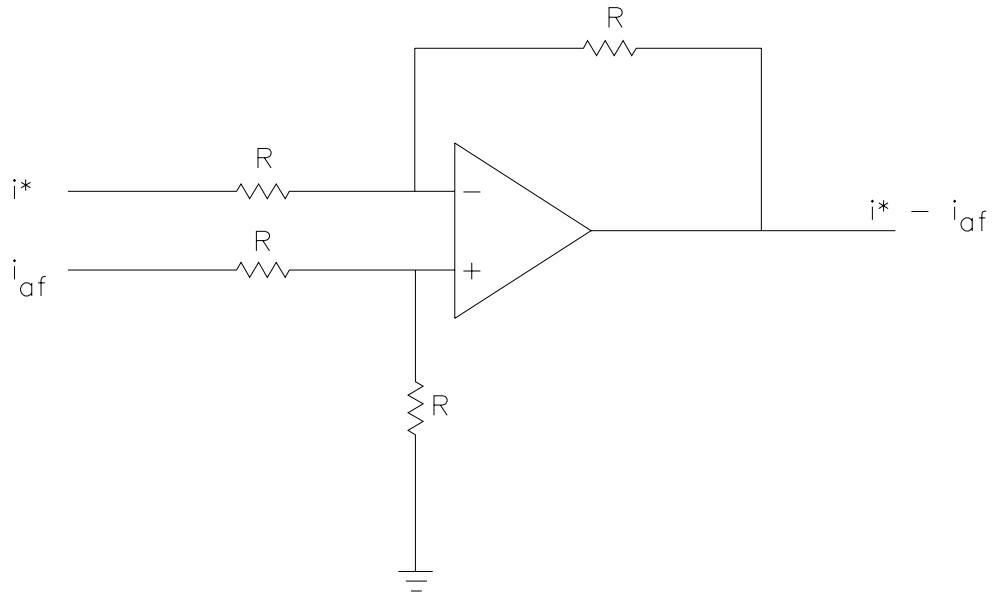

Figure 4.13 – Subtractor Circuit to determine Current Error

Noninverting Terminal :

$$\frac{V - i^*}{R} + \frac{V - 0}{R} = 0$$

$$V\left(\frac{2}{R}\right) = \frac{i^*}{R}$$

$$V = \frac{i^*}{2}$$

Inverting Terminal :

$$\frac{V - i_{amplified\ \ feedback}}{R} + \frac{V - V_O}{R} = 0$$

$$V\left(\frac{2}{R}\right) = \frac{V_O + i_{amplified\ \ feedback}}{R}$$

$$V_O = 2V - i_{amplified\ \ feedback}$$

$$V_O = 2\frac{i^*}{2} - i_{amplified\ \ feedback}$$

$$\underline{\underline{V_O = i^* - i_{amplified\ \ feedback}}}$$

4.2.2.3 Current PI Controller

Once the error had been obtained, it was fed to a Proportional-plus-Integral Controller. In order to effectively tune the PI Controller, the proportional stage was in a separate circuit from the integral stage, and they were added together with a summing circuit. Since all of this control

was analog using discrete components, it was much easier to change gains and tune each stage individually. The gains were chosen to be 10 for the proportional stage and 1 for the integral stage. Once again, all of the stages had to be in a noninverting configuration in order to perform as required. The most challenging section of this controller was designing a noninverting practical integrator since the typical practical integrator is in inverting form. (Practical here meaning that a resistor was also used in addition to a capacitor in order to drain the capacitor and keep the circuit from saturating.) Anti-Windup on the integrator circuit was deemed unnecessary since the application is not high performance; it would just add complexity to the system where it was not needed. The P-stage is shown in figure 4.14, and the I-stage is shown in figure 4.15.

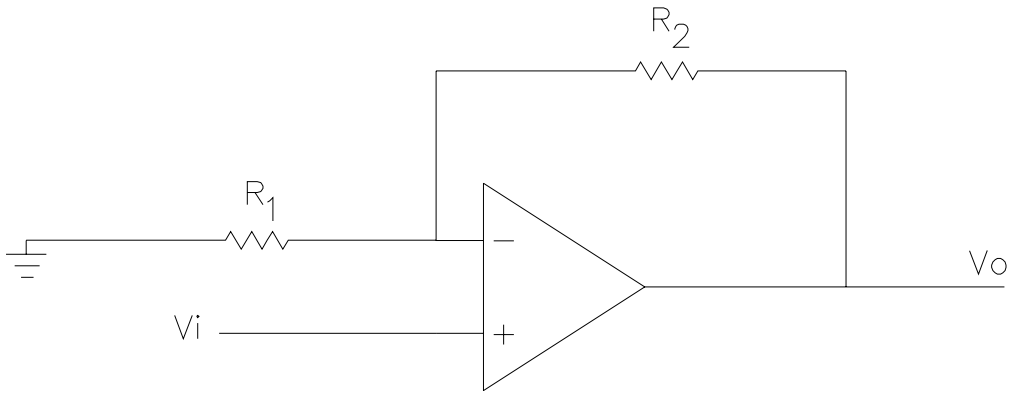

Figure 4.14 – Proportional Gain Stage Circuit for Current PI

Noninverting Terminal :

$$V = V_i$$

Inverting Terminal :

$$\frac{V-0}{R_1}+\frac{V-V_O}{R_2}=0$$

$$V\left(\frac{1}{R_1}+\frac{1}{R_2}\right)=\frac{V_O}{R_2}$$

$$V_O = V_i\left(\frac{R_2}{R_1}+1\right)$$

$$\frac{V_O}{V_i} = A = \frac{R_2}{R_1}+1$$

$$A = 10 = \frac{R_2}{10\ k\Omega}+1 \qquad R_2 = 90\ k\Omega \qquad \underline{\underline{R_1 = 10\ k\Omega \qquad R_2 = 90.9\ k\Omega}}$$

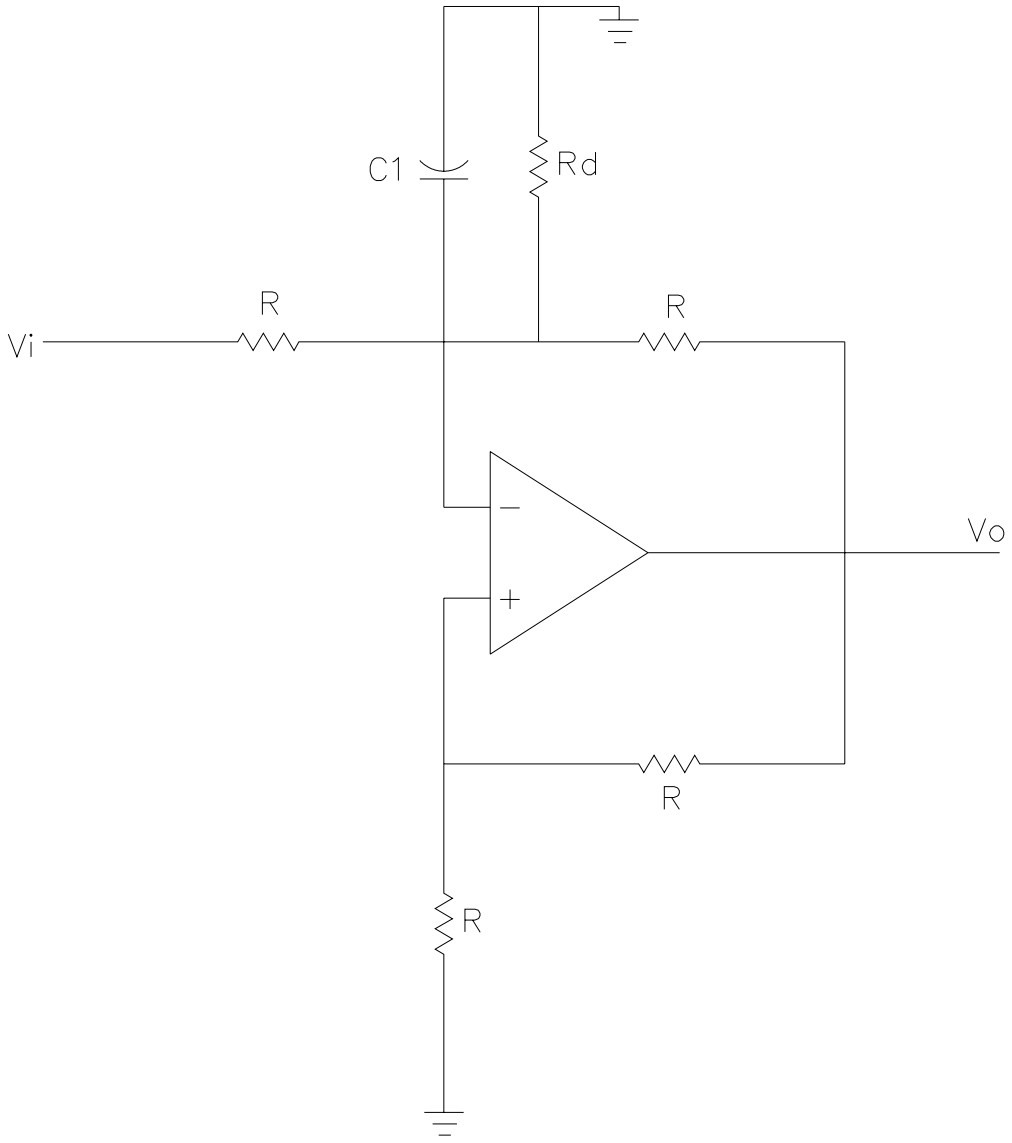

Figure 4.15 – Noninverting Practical Integrator Stage Circuit for Current PI

Noninverting Terminal:

$$\frac{V-0}{R}+\frac{V-V_O}{R}=0$$

$$V\left(\frac{2}{R}\right)=\frac{V_O}{R}$$

$$V=\frac{1}{2}V_O$$

Inverting Terminal:

$$\frac{V-V_i}{R}+\frac{V-0}{\frac{1}{sC}}+\frac{V-V_O}{R}=0$$

$$V\left(\frac{2}{R}+sC\right)-\frac{V_O}{R}=\frac{V_i}{R}$$

$$\frac{V_O}{2}\left(\frac{2}{R}+sC\right)-\frac{V_O}{R}=\frac{V_i}{R}$$

$$\frac{V_O}{2}(sC)=\frac{V_i}{R}$$

$$V_O=V_i\left(\frac{2}{sRC}\right)$$

R_d is added in parallel with C in order to drain charge and not allow saturation. Its design depends on the time constant necessary.

$$R_dC<50\ ms$$

$$R_d<\frac{50\ ms}{1\ \mu F}=50\ k\Omega$$

$$A=1=\frac{2}{RC} \qquad Let\ \ C=1\ \mu F \qquad R=2\ M\Omega$$

$$R=2\ M\Omega \qquad R_d=47\ k\Omega \qquad C=1\ \mu F$$

The summing stage that was used is identical to the summer derived in Section 4.2.2.1 Current Feedback, and it only had a gain of 1. Its form is shown in figure 4.16.

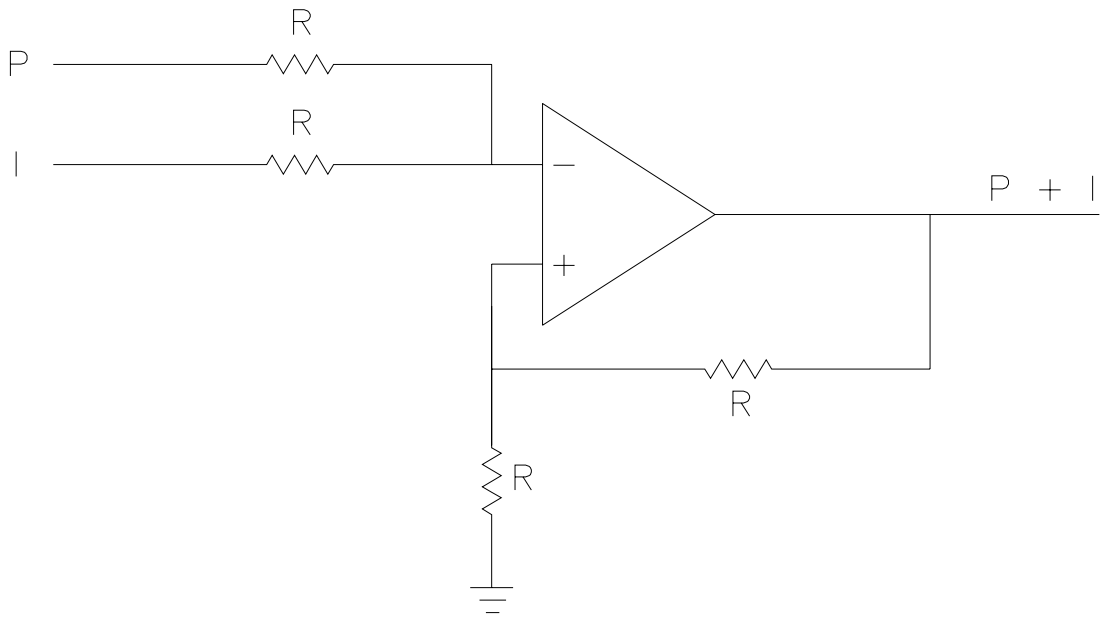

Figure 4.16 – Summing Amplifier for Current PI

4.2.2.4 Current Control Signal Limiter

The duty cycle control signal had to be limited in order to be accurately inputted into the PWM IC. From table 4.2, it can be seen that the maximum control signal that would be accepted by the PWM is 3.53 Volts. But, it is not wise to have full 100 % duty cycle, therefore, it was limited to at most 95 % duty cycle. In order to build a simple, minimum component limiter circuit, a zener diode was used. 3.3 Volt zeners are readily available devices and they would allow the restriction of less than 100 % duty cycle. The output of the PI Controller was fed into a 1 kΩ resistor to limit the current in the 3.3 Volt zener. The output seen across the zener then became the input to the noninverting input terminal of the PWM IC.

4.2.3 Speed Control Loop

Once the form of the gate drive signal and the PWM input signal had been established, the signals needed are derived by working backwards again. The only signal missing was the current command signal that was required to determine if there was current error. This was the signal that will be generated by the speed control loop. The speed control loop, in essence, mirrored the current control loop, and for this reason was simple in its construction, since most

of the design work had already been completed. The form of the speed control loop is shown in figure 4.17. The entire speed control loop logical schematic is shown in Appendix E. The actual wiring diagram for the speed control loop is shown in Appendix F.

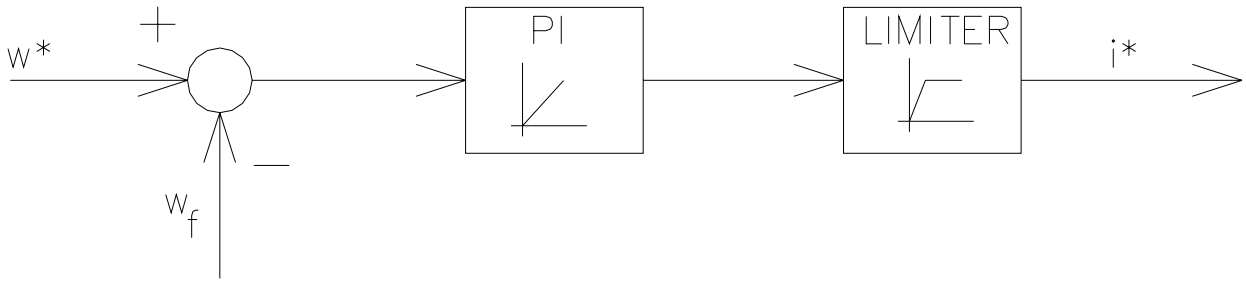

Figure 4.17 – Speed Control Loop Block Diagram

4.2.3.1 Speed Feedback

The first step in current control was to first be aware of the speed at which the machine was operating. There are many ways to determine speed feedback. In this research, an encoder was not available or desired. A simple frequency to voltage converter was used to equate the speed of operation to a voltage level to allow for comparison. The speed was determined by the frequency of the signal from the combination of the Hall sensors that had already been determined in the gate drive signal section. The design of this circuit involving the frequency to voltage converter was the most time consuming aspect of the entire speed loop, in spite of an excellent application reference. In order to accurately compare the command to the feedback, the frequency to voltage converter had to be able to output 10 Volts when the machine was at full voltage and full speed. This allowed for no error to be generated when the machine was at full voltage and full speed when a full command was given. In order to allow for 10 Volts, the frequency at full speed had to be determined and designed around. It was been seen in the gate drive signal section, that it took four pulse trains to complete one revolution. One pulse train segment was equal to one period. Therefore, the frequency could be determined from this knowledge and the fact that at full speed the machine rotates at 10,000 revolutions per minute.

$$\frac{1}{4}\ revolution = \frac{10{,}000\ revolutions}{minute} T$$

$$T = 25\,\mu\min\left(\frac{60\ s}{1\ \min}\right) = 1.5\ ms$$

$$f = \frac{1}{T} = \frac{1}{1.5\ ms} = 667\ Hz$$

The highest frequency achievable is 667 Hz. Now, this had to be equated to the voltage, and the Hertz per Volts ratio was determined.

$$\frac{x\ Hz}{667\ Hz} = \frac{1\ V}{10\ V}$$

$$x\ Hz = (667\ Hz)(0.1\ V)$$

$$\frac{Hz}{V} = \frac{66.7\ Hz}{1\ V}$$

With this value known, the datasheet for the LM2907 frequency to voltage converter gives the follow equation:

$$V_O = V_{cc} f_{in} C_1 R_1$$

Every quantity except the values of the resistor and capacitor were known in this equation. Since resistors have more standard sizes than capacitors, the value of the capacitor was set and the value of the resistor was designed. The capacitor was set to 0.01 μF.

$$V_O = V_{cc} f_{in} C_1 R_1$$

$$10\ V = (12\ V)(667\ Hz)(0.01\ \mu F) R_1$$

$$R_1 = 125\ k\Omega$$

$$\underline{\underline{R_1 = 120\ k\Omega\ in\ series\ with\ a\ 4.99\ k\Omega}}$$

There were other concerns with this chip though. The output current on pin 3 was internally fixed; therefore, the output voltage divided by R_1 had to be less than or equal to that value. I_{3MIN} was given in the LM2907 datasheet.

$$R_1 \geq \frac{V_O}{I_{3\,MIN}} = \frac{10\ V}{150\ \mu A} = 67\ k\Omega \qquad R_1 = 125\ k\Omega \quad \surd$$

Also, the maximum attainable frequency had to be evaluated. I_2 was given in the LM2907 datasheet.

$$f_{MAX} = \frac{I_2}{C_1 V_{cc}} = \frac{190\ \mu A}{(0.01\ \mu F)(12\ V)} = 1583\ Hz \qquad f_{MAX} = 667\ Hz \quad \surd$$

As one final concern and design point, the ripple content of the output had to be examined. The ripple content was determined by one final design component, a capacitor. But, this capacitor also affected the response time, so a compromise had to be reached. A ripple of less than 0.01 Volt ripple was required. That equated to approximately 10 rpm.

$$V_{Ripple} = \frac{V_{cc}}{2}\left(\frac{C_1}{C_2}\right)\left(1 - \frac{V_{cc} f_{in} C_1}{I_2}\right) pk - pk = 0.01\ V$$

$$C_2 = \frac{(12\ V)(0.01\ \mu F)}{2(0.01\ V)}\left(1 - \frac{(12\ V)(0.01\ \mu F)(667\ Hz)}{190\ \mu A}\right)$$

$$C_2 = 3.47\ \mu F$$

$$\underline{\underline{C_2 = 4.7\ \mu F}} \Rightarrow V_{Ripple} = 0.007\ V\ \ pk - pk$$

With all of the components required designed for, the circuit was implemented and tested. But, it was found that the circuit did not work. It was tested using a signal generator for the input, and it was not until a dc offset was added did the circuit perform as expected. The application notes are clear in that the reference for all input signals must be ground or below ground. The sensor output signals were from ground to positive 12 Volts. The fact that the circuit did not function with the given input signal was baffling, until a survey of the noise was performed. The noise was not large enough to be of any consequence in any other function; however it was sufficient to keep this circuit from performing as expected. In reviewing more application notes on the LM2907, it was discovered that it was possible to use input signals that were referenced above ground with a special configuration involving a reference voltage put to the inverting terminal of the LM2907 (14 pin version only) instead of tying it to ground. A voltage divider involving a potentiometer was designed to supply a reference voltage anywhere from zero to 10 volts. Once this was done, the circuit performed up to expectations. Its connections are shown in figure 4.18.

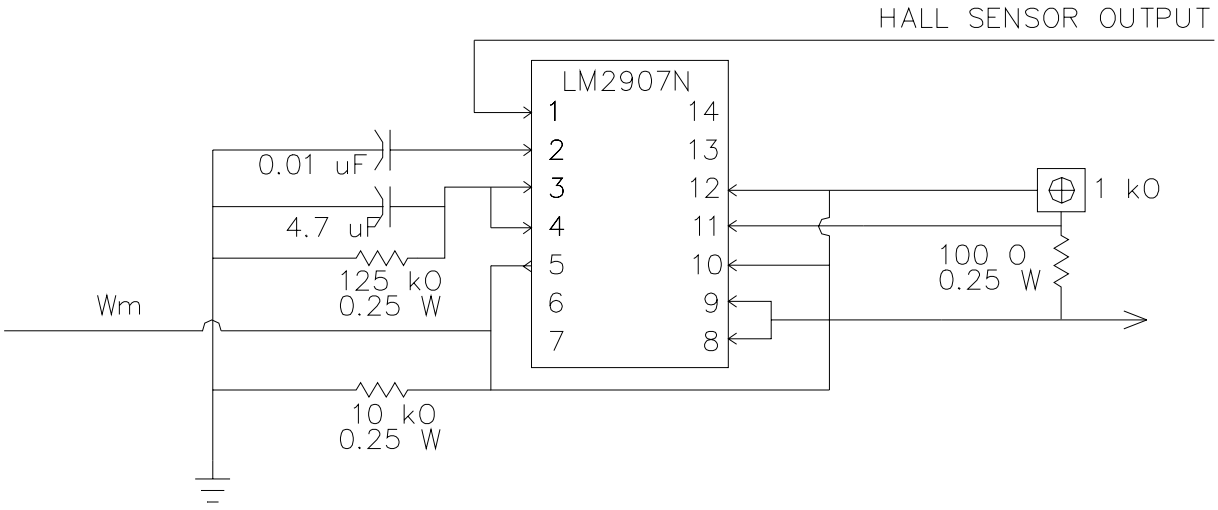

Figure 4.18 – Frequency to Voltage Converter Connections

At this point, the feedback was ready to be compared to the reference to give an error and generate a current command signal.

4.2.3.2 Speed Command Generation

The speed command generation involved a simple circuit that was a voltage divider to provide 10 Volts at full command and zero Volts at no command. A 200 Ω resistor was placed in series with a 1 kΩ Linear Taper Speed Potentiometer (Potentiometer involving a knob to allow for easy control rather than a screwdriver type adjustment). A 12 Volt supply was connected, and the output was drawn from the adjustable pin of the potentiometer. This allowed for a full zero to 10 Volt command.

4.2.3.3 Speed Error Determination

In order to determine the error, the feedback must be subtracted from the command. This was performed by way of a subtractor circuit with a gain of 1 just as in the current control loop. The design justification is the same as the previous section and will not be derived again here. Since all of the resistors are of the same value, the equations work out so the output in not dependent on their value; therefore, the standard value of 100 kΩ was chosen so as to avoid the same offset discovered in the current control loop. The form of the subtractor circuit used here is shown in figure 4.19.

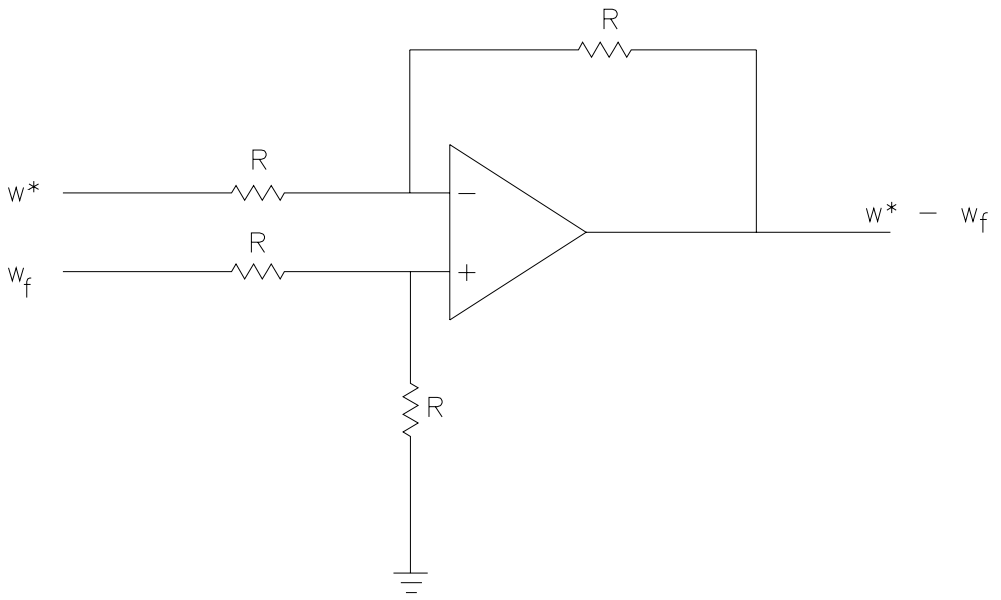

Figure 4.19 – Subtractor Circuit to determine Speed Error

4.2.3.4 Speed PI Controller

Once the error had been obtained, it was fed to a Proportional-plus-Integral Controller just as in the current control loop. In order to effectively tune the PI Controller, the proportional stage was in a separate circuit from the integral stage, and they were added together with a summing circuit. Since all of this control stage was analog using discrete components, it was much easier to change gains and tune each stage individually. The gains again were chosen to be 10 for the proportional stage and 1 for the integral stage. Once again, all of the stages had to be in a noninverting configuration in order to perform as required. Just as in the current control loop, anti-windup on the integrator circuit was deemed unnecessary since the application is not high performance; it would just add complexity to the system where it was not needed. The form of the proportional gain stage and the integral gain stage are shown in figures 4.20 and 4.21 respectively. The summing stage that was used is identical to the summer derived in Section 4.2.2.1 Current Feedback. Its form is shown in figure 4.22.

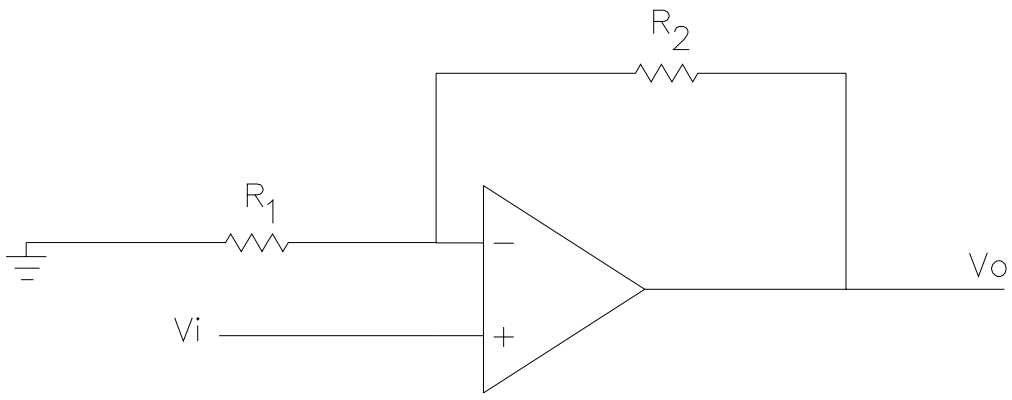

Figure 4.20 – Proportional Gain Stage Circuit for Speed PI

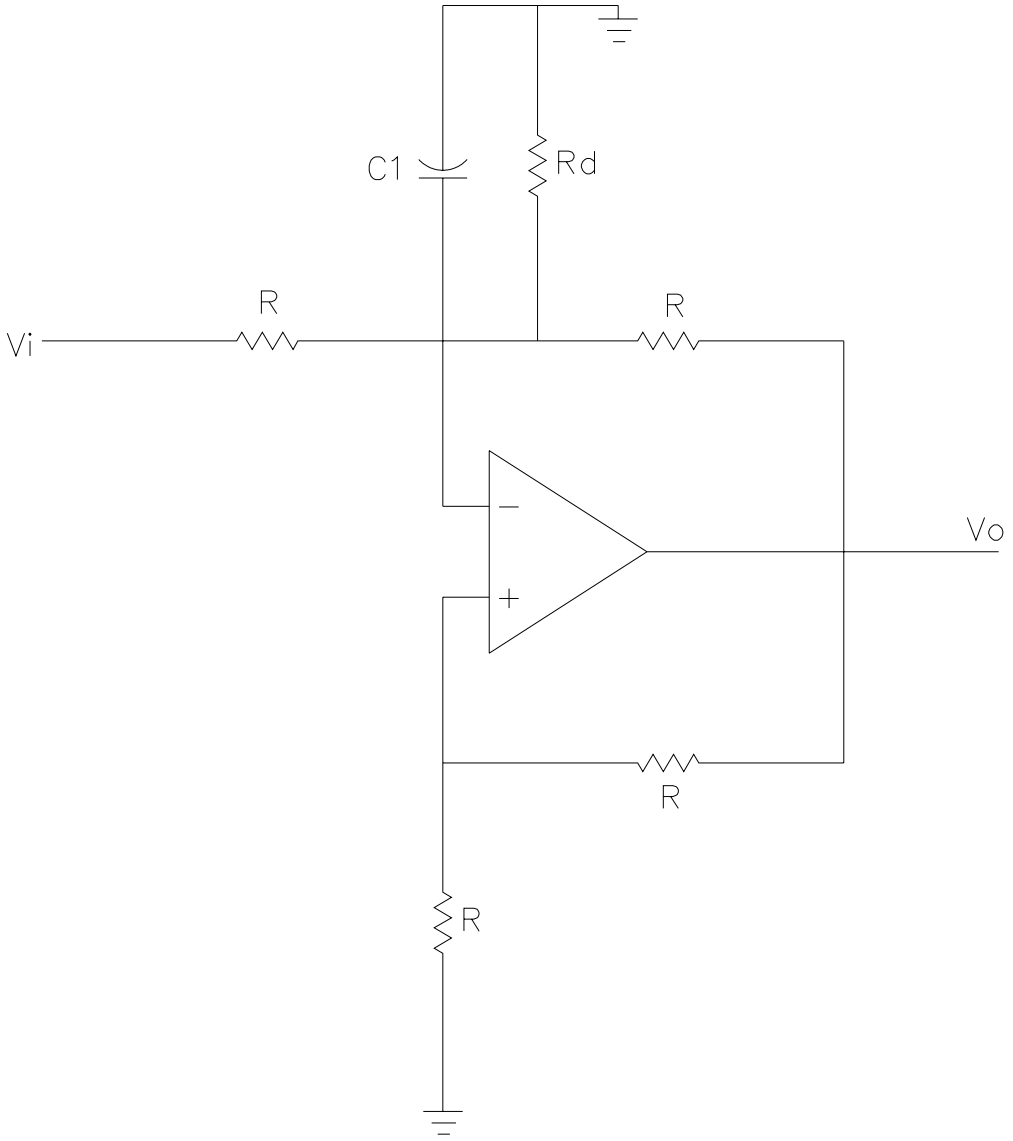

Figure 4.21 – Noninverting Practical Integrator Stage Circuit for Speed PI

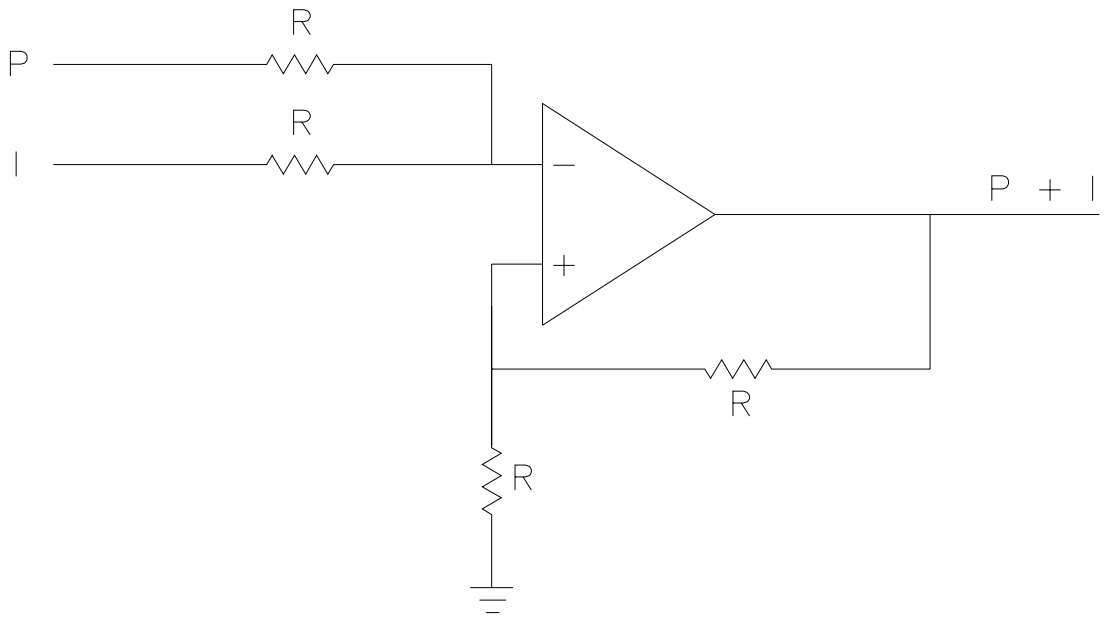

Figure 4.22 – Summing Amplifier for Speed PI

4.2.3.4 Speed Control Signal Limiter

The current command signal had to be limited in order to be accurately compared to the current feedback. From the design of the current feedback amplification, it is seen that the maximum voltage allowed for the current command in order to have zero error with the signals match was 4.7 Volts. In order to build a simple, minimum component limiter circuit, a zener diode was used. 4.7 Volt zeners are readily available devices. The output of the PI Controller was fed into a 1 kΩ resistor to limit the current in the 4.7 Volt zener. The output seen across the zener then became the input to the noninverting input terminal of the subtractor circuit that determined the current error.

4.3 Construction and Connection

Each stage was constructed just as it was designed. First the PWM IC circuit was built and tested to ensure that the output was a signal of varying duty cycle given a certain input. Then the hall sensors and logic gates were connected to allow for proper gate drive signals. This was tested and checked to make sure that the desired signal was achieved. Next, the current

control loop was built and closed. The feedback was confirmed to make sure that the loop was indeed closed. Finally, the speed loop was built and closed. The speed feedback was then confirmed to ensure that the loop was closed once again. With the closing of this last loop, a command was given and the feedback was monitored. When the two signals matched, the drive system was complete.

Chapter 5. Experimental Results and Evaluation

5.1 Experimental Setup

Since there are many ways of connecting the machine windings, some clarifications must be made as to the experimental setup for this research. The main windings were connected in series then connected to the converter circuit. The interpoles were connected in series in two sets of pairs. Then they were introduced into the converter circuit separately. Since the interpoles were not all connected in series, this would allow for bi-directional starting. The winding diagrams for the main and interpole windings are shown in figure 5.1. For this thesis, only uni-directional operation was considered; therefore, one set of the interpoles was not connected.

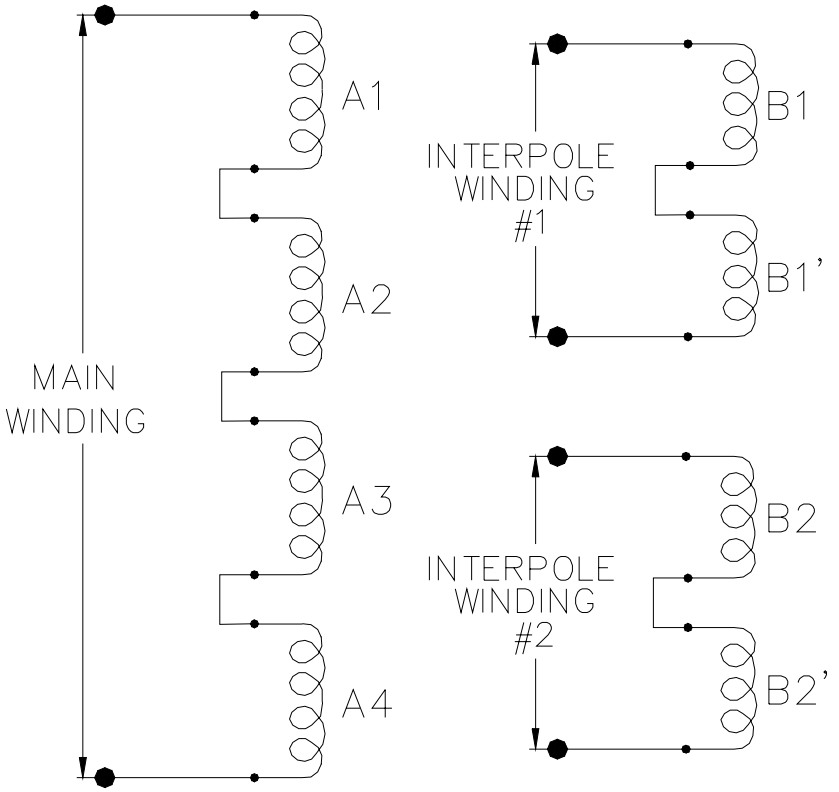

Figure 5.1 – Proposed Wiring Schematic

3177 Allegro Microsystems Hall effect sensors were used to obtain position information. These sensors are attached as described in Section 4.2.1 PWM Control and Gate Drive Signal.

5.2 Experimental Results

The experimental results of this research are contained in this section. All measurements were taken at 60 Volts AC at a maximum speed of 6800 RPM.

First, the Hall Sensor Scheme is examined. The outputs of the two hall sensors and their respective combination through an exclusive OR gate is given in figure 5.2. From this graph, it can be seen that the hall sensors give an output with the passing of a magnet (high for a north pole and low for a south pole). This corresponds to two high signals and two low signals for each rotation. From the staggering of the pulses, it can be noted that the sensors are 45 degrees apart, just as specified in the mechanical diagram in figure 4.2. When these two signals are combined by and exclusive OR, four pulses are generated with each single revolution.

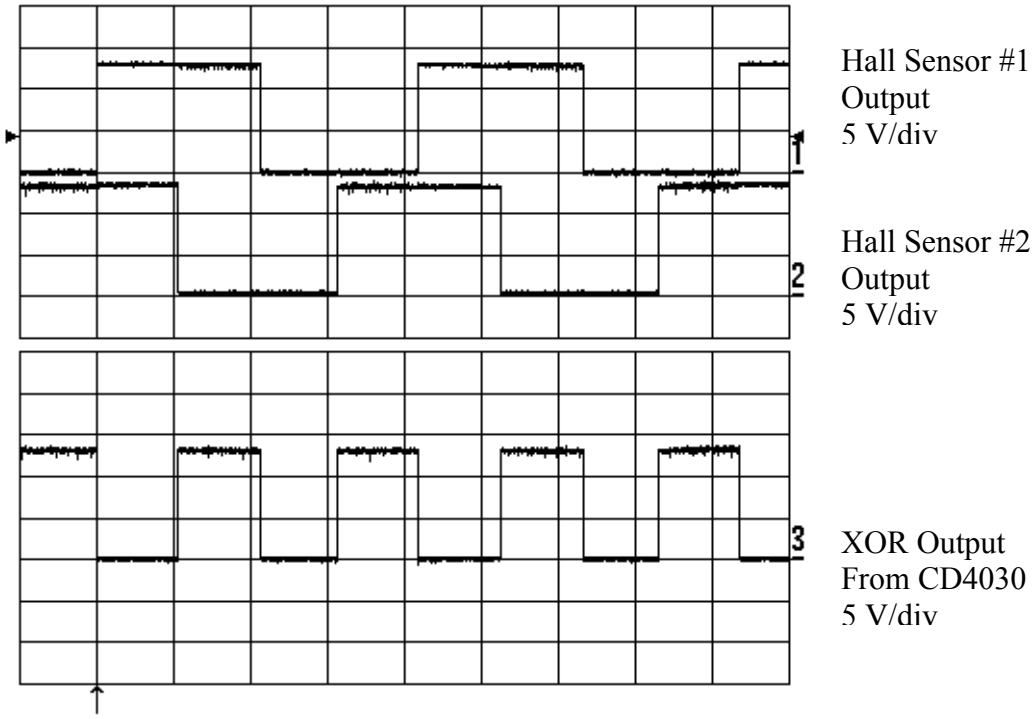

Figure 5.2 – Hall Sensor Outputs and Combination Output

Next, the Gate Drive Signal logic is examined. The hall sensor XOR output, PWM output and the output of the AND gate to the gate drive are given in figure 5.3. From this graph, it can be seen that the level of the hall sensor XOR output is translated to the PWM pulses by the AND to give the IGBT Gate Drive Signal. When the XOR is low, the drive signal is also low, but when the XOR is high, the drive signal is a pattern of pulses with the duty cycle determined by the PWM circuit.

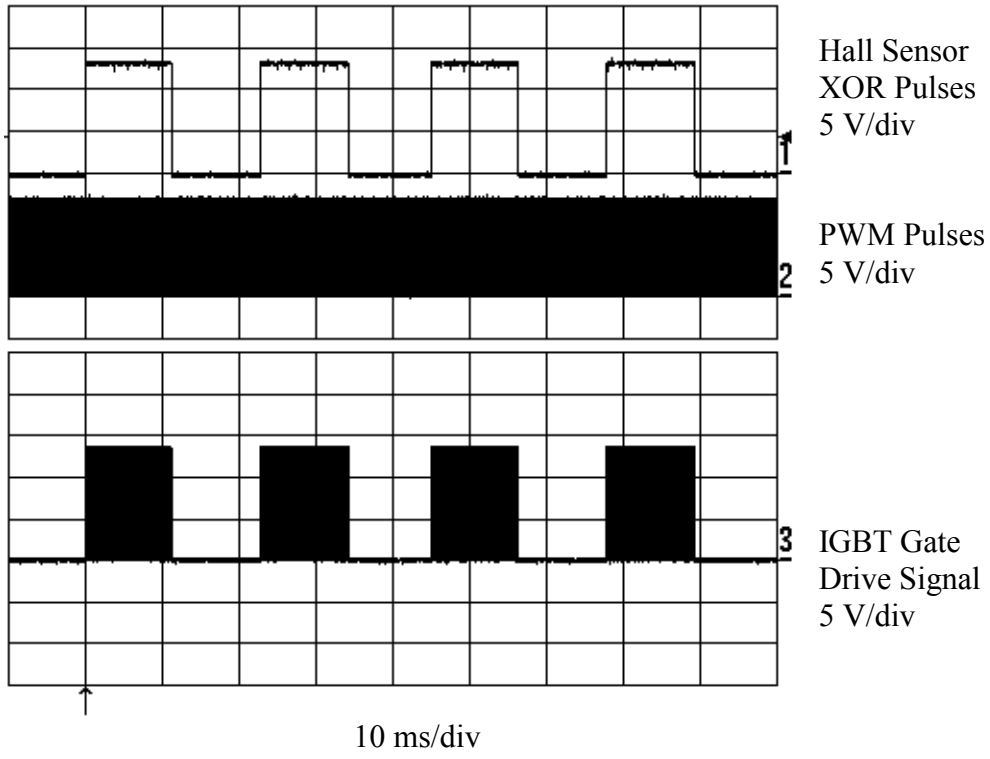

Figure 5.3 – Gate Drive Signal from PWM and Hall Sensor Pulses

Next, the speed command versus the speed feedback is analyzed and verified in figure 5.4. Both plots are on the same time division scale as well as the same amplitude division scale. The top curve represents the speed command. This command varies between zero and two Volts in approximately nine seconds, which represents a final command speed of 2000 RPM. The waveform is slightly jumpy since, the reference is given by way of a speed knob, and the operator's hands are not capable of giving a perfect ramp as is a command given by a DSP. The

bottom curve represents the speed feedback. This curve varies between zero and two Volts in slightly less than ten seconds. This signal is slightly noisy, which is to be expected. It can be seen that this feedback follows the command almost exactly. It even plateaus as the command plateaus. Once the command reaches its steady value, the feedback also reaches the equivalent steady value, and it remains there as long as the command does.

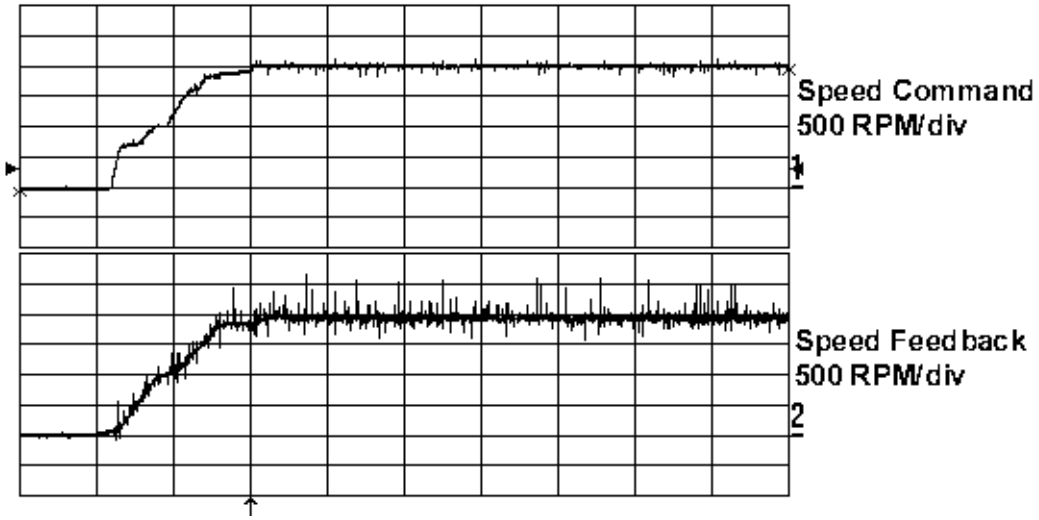

Figure 5.4 – Speed Feedback and Speed Command

Next, the current command versus the current feedback is analyzed and verified in figure 5.5. The top curve represents the current command. This command can vary between zero and 4.7 Volts. Here it is seen that the command it constantly at 4.7 Volts; this is due to the fact that the speed was at full command and the voltage was not at a full 120 Volts AC. It was impossible for the current to reach its full eight Amperes; therefore, the command was constantly trying to push for eight Amperes. The command is a straight DC level due to the structure of the speed control loop. The bottom curve represents the current feedback, which is a view of the current in the main windings.

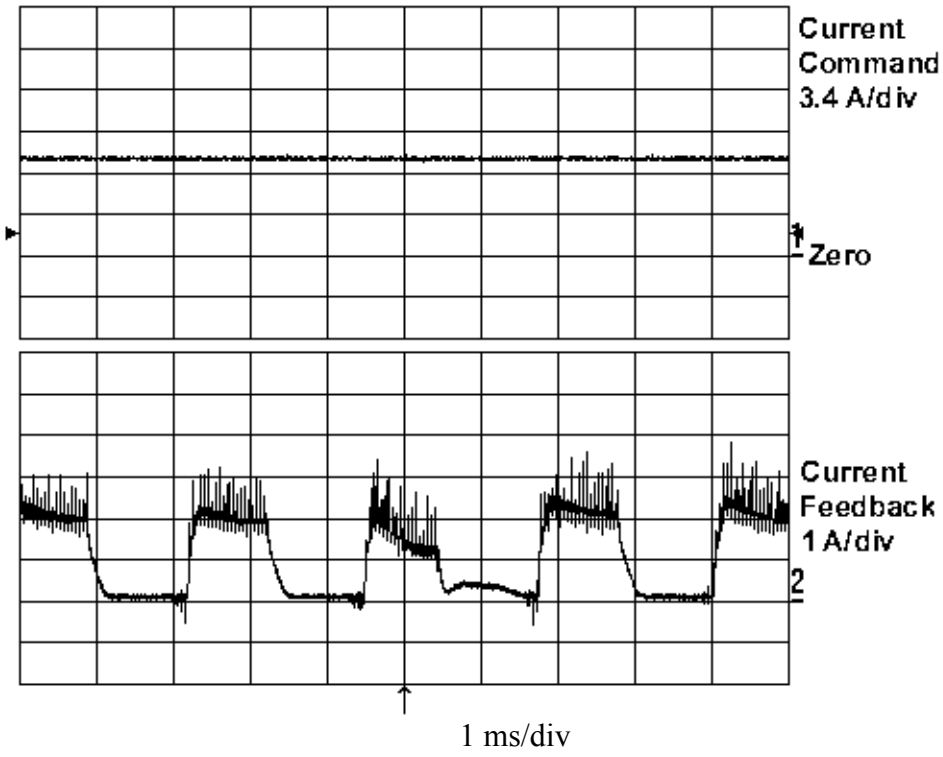

Figure 5.5 – Current Feedback and Current Command

At this point, it is important to expand the view of the current in the main windings as is done in figure 5.6. This expanded view demonstrates the switching found in the current waveform, which is expected with the drive signal being dependent on a PWM signal. This graph demonstrates that the drive is performing as expected.

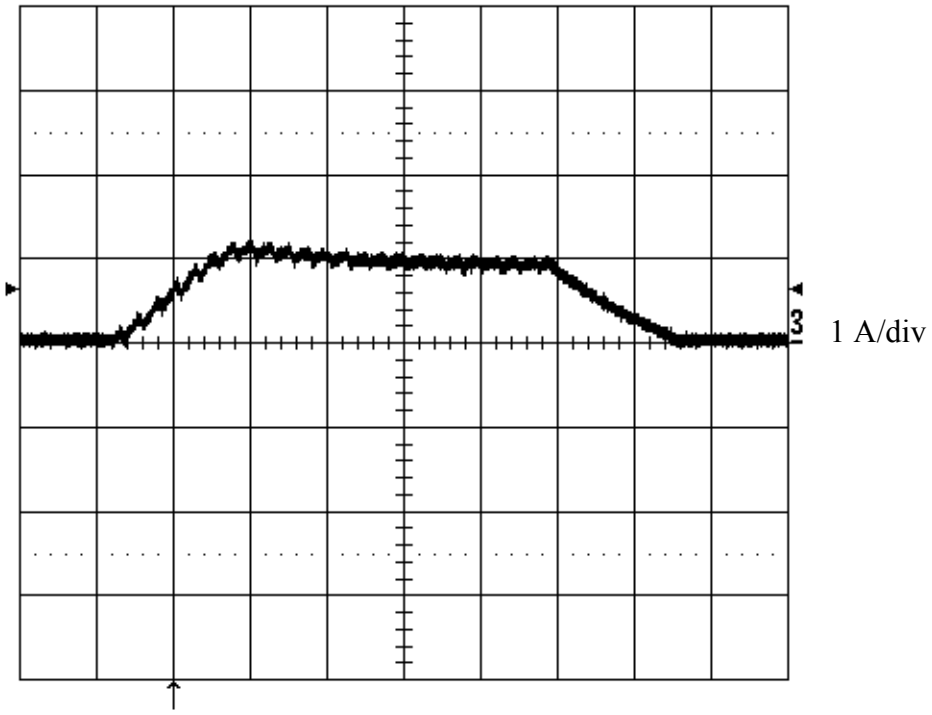

Figure 5.6 – Main Winding Current Expanded to show Switching

Next, the currents in the main and auxiliary windings are examined in figures 5.7 and 5.8. These two plots are of the same quantities but the first is with a snubber capacitor of one microfarad and the second is with a snubber capacitor of 4.7 microfarads. The top curve in the first graph is the current in the auxiliary windings and the bottom curve is of the current in the main windings. The top curve in figure 40 is of the current in the main windings and the bottom is of the current in the auxiliary windings. Both of these graphs are displayed here to show the tradeoffs with the design of the snubber capacitor. From the first graph, it can be seen that the main current waveform is much more attractive than that of the main current in figure 5.7. It drops almost immediately to zero during the turn off time, so negative torque will not be produced and audible noise will be reduced. But, when attention is turned to the auxiliary current waveform, it is seen that the auxiliary has only minimal current during the off time of the main windings. This will be a problem with the issue of self-starting since their must be current in the auxiliary in order to pull the rotor to the unaligned position. So, it appears that the 4.7 microfarad capacitor would be a better fit for the snubber capacitor since there is significant

current in the auxiliary winding during the off time. The only problem is that the main winding current is not allowed to fall to zero immediately in the off time, which will produce negative torque and possibly more audible noise.

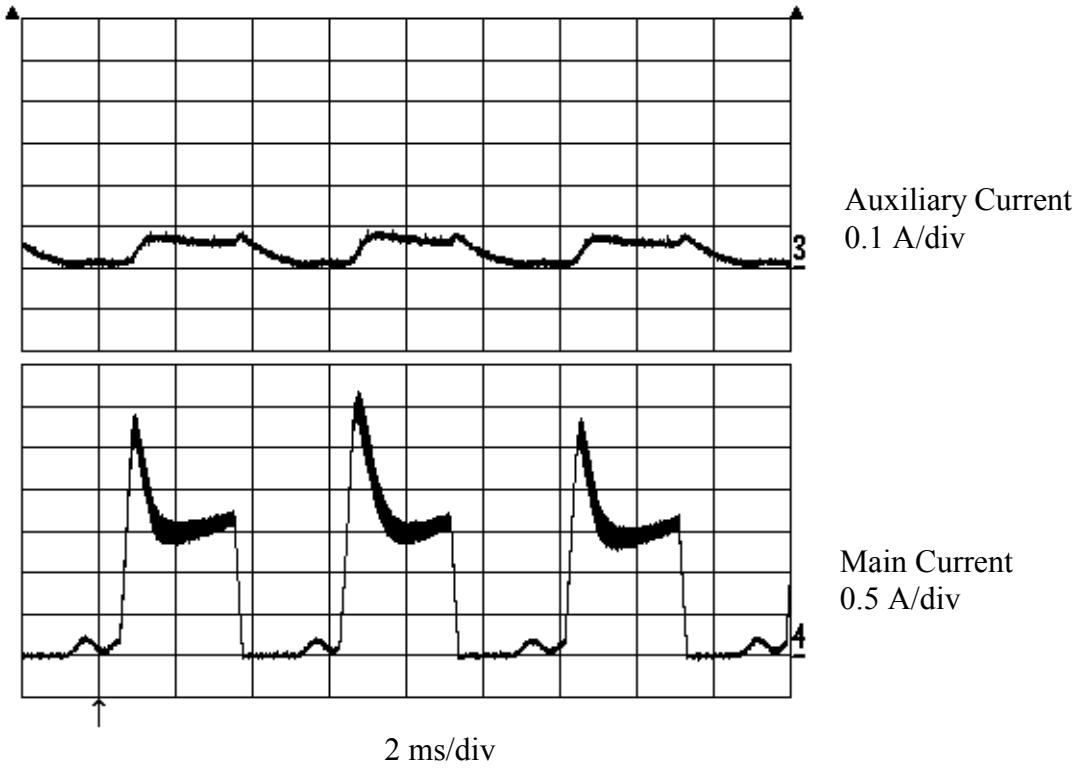

Figure 5.7 – Main Winding Current and Auxiliary Winding Current with 1 microfarad cap

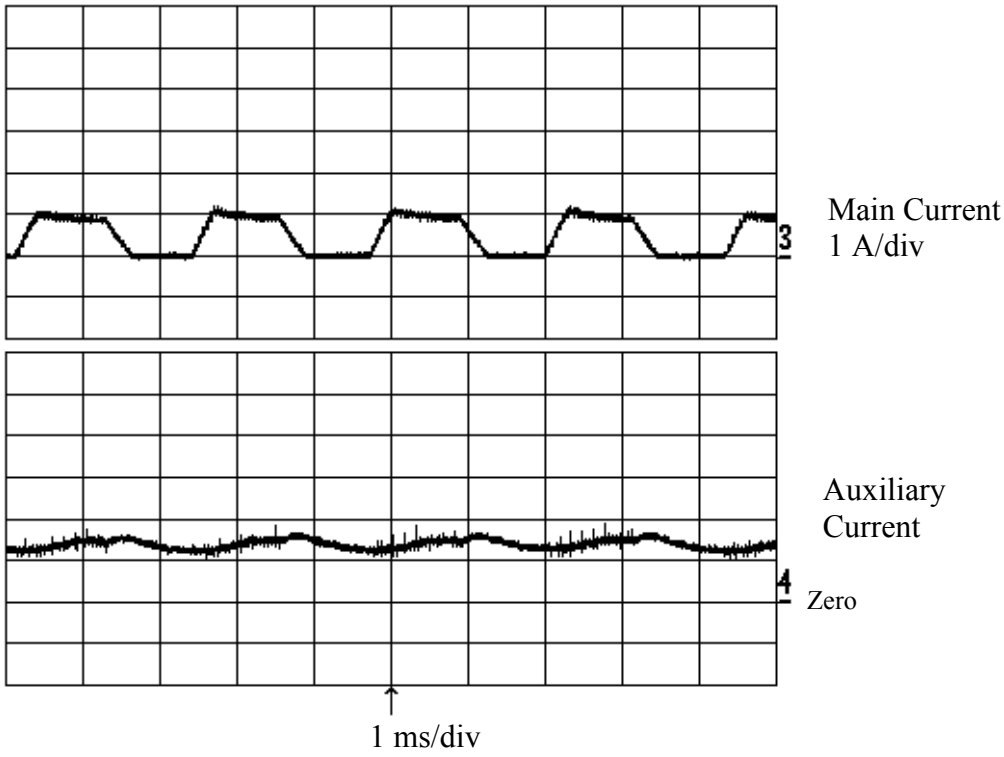

Figure 5.8 – Main Winding Current and Auxiliary Winding Current with 4.7 microfarad cap

Next, the voltage for the main windings is shown is figure 5.9 and 5.10. These measurements were taken with an AC voltage of approximately 60 V, which leads to the DC Link voltage of approximately 84 Volts, which is what the maximum is very near. These graphs show the switching of the voltage involved in the on time of the current. Figure 41 shows the switching very clearly. Then at the end of the on time, the full negative voltage is applied and then falls to zero, when there is no current.

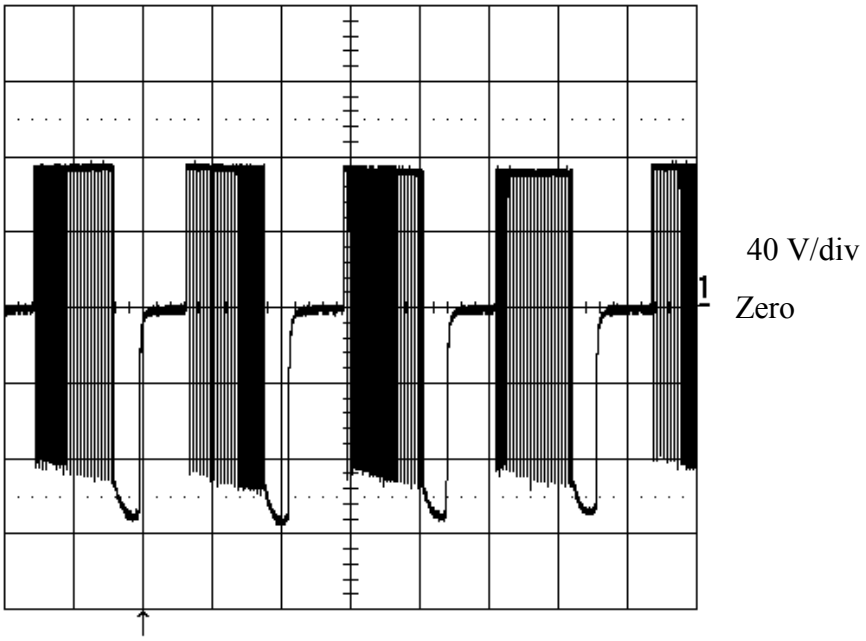

Figure 5.9 – Main Winding Voltage

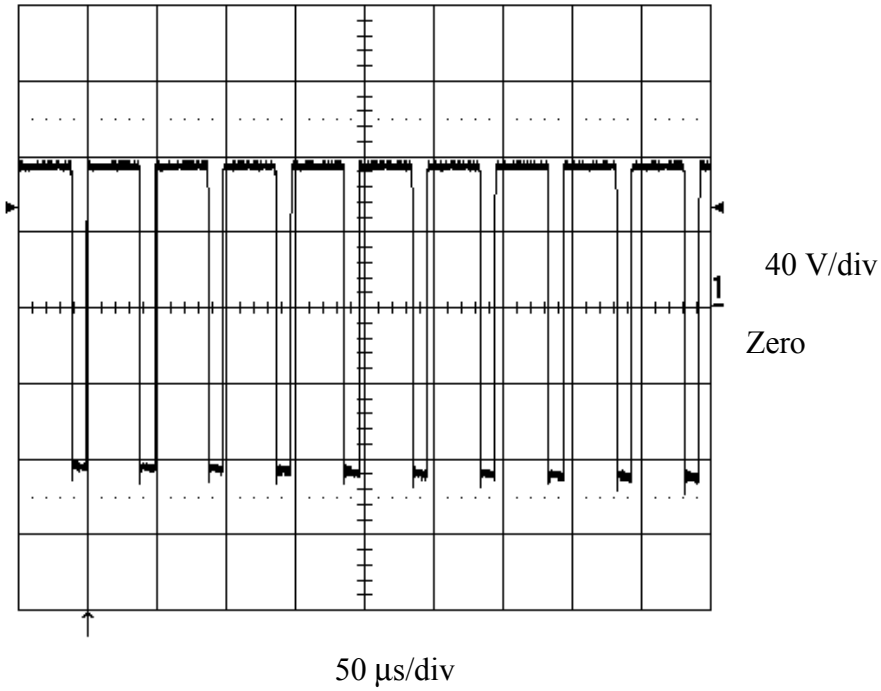

Figure 5.10 – Main Winding Voltage Expanded View to show Pulsing

The next set of graphs show the snubber capacitor voltage and the main winding current for reference in figure 5.11 and the expanded view of the snubber capacitor voltage in figure 5.12. The first figure demonstrates the charging of the capacitor during the on time of the main winding current and the discharge of the capacitor energy during the off time. This discharge energy is applied to the auxiliary windings in order to provide the necessary current. The expanded view of figure 5.12 shows more in depth the charging of the capacitor with its switching and then the discharge through the auxiliaries. It must be noted that the zero for this waveform is not on the scale; in order for the waveform to be expanded enough to show the distinct charging pattern, the zero was shifted off the screen. The swift charge after the switching charge pattern can be attributed to the fact that the waveform had entered the off time of the main winding current, but the current in the mains had not drained fully yet. It was then that the current charged the capacitor to this level in order to drain itself to zero before the capacitor started to drain through the auxiliary winding.

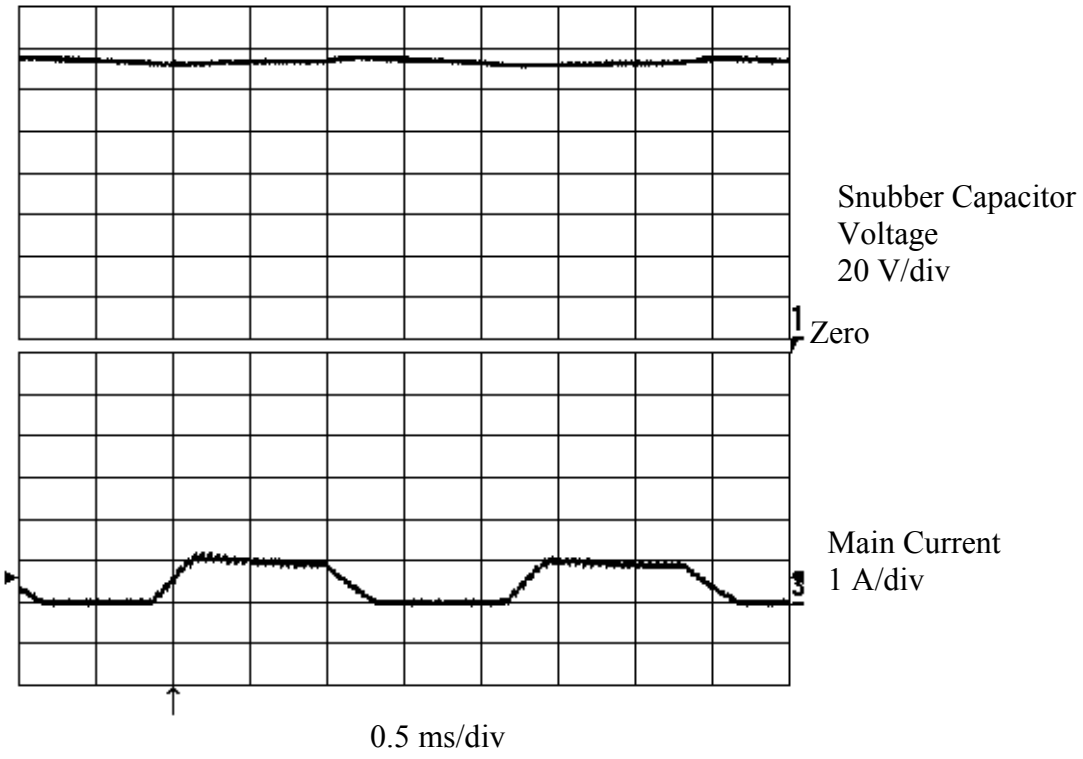

Figure 5.11 – Snubber Capacitor Voltage and Main Winding Current

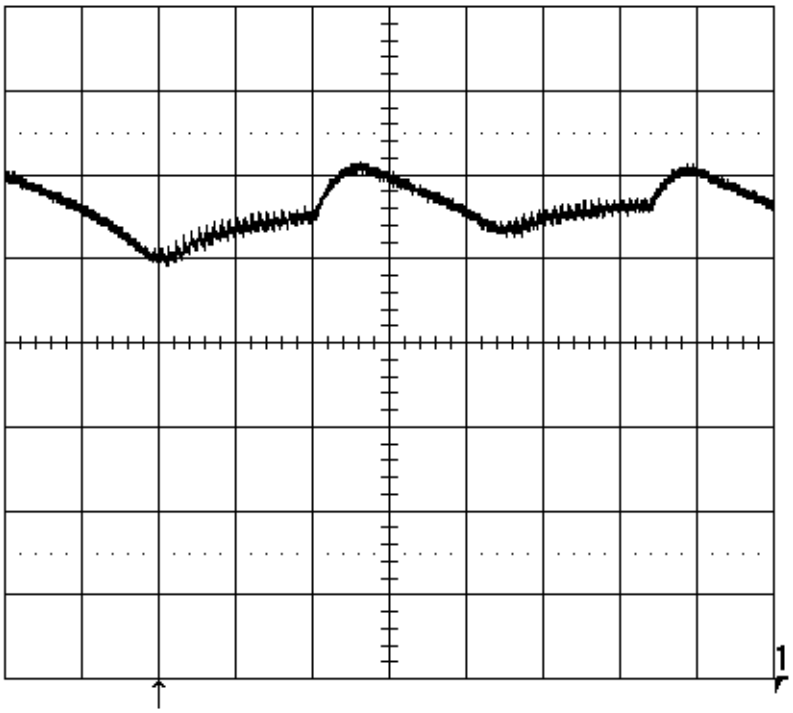

Figure 5.12 – Expanded View of the Snubber Capacitor Voltage

5.3 Evaluation

Overall, this research work reached the end result that was to be expected. The system performs to expectations. At full voltage, the machine is capable of reaching a speed of approximately 10,000 rpm. It reliably operates at the speed given by the operator. Although, the machine was not officially connected to known load, it was loaded slightly by touch of hand, and it performed as expected.

It is recommended that in future research with this machine that an anchoring mechanism and an enclosure for the machine be built for safety concerns. Then a load may be attached and tested fully. An enclosure should be required at speeds in excess of 5,000 rpm for if a rotor fixture magnet came loose and was to fly out of the machine, the results could be dangerous. This enclosure must also allow for proper air flow in order to keep the machine cool.

Chapter 6. Conclusions

6.1 Summary

This thesis describes a novel single phase SRM, an original converter to drive the machine, and a controller to obtain a speed controlled drive system out of the single-phase SRM. The research results are original and depart significantly from the single-phase SRM and drives systems available in the literature and given in patents. The following conclusions are derived from the research results of the thesis:

(i) Verification of analytical inductance results from finite element analysis by experimental methods is given.

(ii) Current sensing, derivation of a logic power supply and a controller circuit and its realization with least expense and ready for use in industrial applications are developed and given.

(iii) In order to eliminate external expensive current sensors, simple resistor based current sensing scheme is introduced as there is no need for isolation required between the power circuit and control circuit with the novel converter topology.

(iv) A simple, inexpensive frequency to voltage converter is employed instead of using an encoder to obtain speed feedback information.

(v) A simple minimum component, analog controller circuit has been developed and recognized to implement a speed controlled drive.

(vi) The machine, converter and controller are developed and tested in the laboratory to prove the feasibility of the proposed single phase SRM drive system.

All of the above clearly constitute a set of original contributions in the field of SRM drive systems. The author of this thesis directly contributed to the electronics design of the converter and controller. Also, the author implemented the system in its entirety and experimentally verified its operation at a wide range of speed.

6.2 Possible Applications

Many applications are possible with this drive system. The most obvious of applications are for pump and fan loads. This drive is well suited for submersible pump or fan applications. Also, a well-matched application would be for power tools that require variable speed operations such as drills or drivers.

6.3 Recommendations for Future Work

Possible avenues of future research could include acoustic noise control for extremely high-speed operation, sensorless operation, bi-directional operation, analysis of different winding connections, as well as multiple phase operation. Also, the tools for sensorless operation are provided within this thesis, but true sensorless operation is not achieved. Simple implementation of a new control methodology could provide for further reduced cost. Also, with the machine configuration, bi-directional operation is possible but is not realized in this thesis. Furthermore, with the selection of an appropriate converter, four-quadrant operation is possible.

References

[1] C. C. Chan, "Single-phase switched reluctance motors," IEE Proc.-B, vol. 134, no. 1, pp. 53-56, Jan. 1987.

[2] J. M. Stephenson and G. C. Jenkinson, "Single-phase switched reluctance motor design," IEE Proc. Electr. Power Appl., vol. 147, no. 2, pp. 131-139, Mar. 2000.

[3] J. Y. Lim, H. S. Kim, J. Y. Oh, D. H. Cheong, and J. C. Kim, "A performance of single phase switched reluctance motor having both radial and axial air gap," in Proc. IECON, 1998, pp. 905-910.

[4] S. Chan and H. R. Bolton, "Performance enhancement of single-phase switched-reluctance motor by DC link voltage boosting," IEE Proc.-B, vol. 140, no. 5, pp. 316-322, Sept. 1993.

[5] M. Barnes and C. Pollock, "Power converter for single phase switched reluctance motors," Electronic Letters, vol. 31, no. 25, pp. 2137-2138, Dec. 1995.

[6] M. Barnes and C. Pollock, "Selecting power electronic converters for single phase switched reluctance motors," in Proc. Power Electronics and Variable Speed Drives, 1998, pp. 527-531.

[7] E. Buchan and N. Fulton, "Apparatus and method for starting a single-phase variable reluctance motor," US Patent number 5,753,984, May 19, 1998.

[8] J. Stephenson, "Apparatus and method for starting a single-phase variable reluctance motor," US Patent number 5,808,389, Sept. 15, 1998.

[9] G. Horst, "Shifted Pole Single Phase Variable Reluctance Motor," US Patent number 5,294,856, Mar. 15, 1994.

[10] R. Krishnan and P. Materu, “Design of a Single-Switch-Per-Phase Converter for Switched Reluctance Motor Drives,” in Proc. IECON, 1988, pp. 773-779.

[11] R. Krishnan, A. M. Staley, and K. Sitapati, “A Novel Single-Phase Switched Reluctance Motor Drive System,” in Proc. IECON, 2001.

Appendices

Appendix A – Equipment Listing and Cost Analysis

Part Number	Part Description	Manufacturer	Number Required	Unit Cost	Total Cost
Board	Prototype Circuit Board	Vector Electronic Company	1	25.36	25.36
BTB	Barrier Terminal Block	Cinch	1	3.37	3.37
TB	(2 pin) Terminal Blocks	Thomas & Betts	1	1.72	1.72
TB	(2 Pin) Terminal Blocks	Thomas & Betts	6	1.17	7.02
KBL04	400 V, 4 A Bridge Rectifier	General Semiconductor	1	2.07	2.07
UGN3177UA	Hall Effect Latch	Allegro Microsystems	2	0.90	1.80
G4PC40U	IGBT	International Rectifier	1	5.12	5.12
40EPF04	Power Diode	International Rectifier	1	3.30	3.30
LM324AN	Quad Op Amp	Texas Instruments	3	0.68	2.04
LM2907N	Frequency to Voltage Converter	National Semiconductor	1	2.02	2.02
UC3524N	Advanced Regulating Pulse Width Modulator	Texas Instruments	1	1.93	1.93
CD4081BE	CMOS Quad “AND” Gate	Texas Instruments	1	0.45	0.45
CD4030BE	CMOS Quad “XOR” Gate	Texas Instruments	1	0.66	0.66
1000 µF, 250 V	Aluminum Electrolytic Capacitor	Panasonic	1	8.09	8.09
47 µF, 35 V	Aluminum Electrolytic Capacitor	Panasonic	1	0.28	0.28
4.7 µF, 450 V	Aluminum Electrolytic Capacitor	Panasonic	1	1.19	1.19

0.01 µF	Monolithic Capacitor	Panasonic	3	0.44	1.32
1 µF	Monolithic Capacitor	Panasonic	2	3.12	6.24
4.7 µF	Tantalum Capacitor	Panasonic	1	0.56	0.56
1N4728	3.3 V Zener	Diodes, Inc.	1	0.36	0.36
1N4732	4.7 V Zener	Diodes, Inc.	1	0.36	0.36
1N5242	12 V, ½ W Zener	Diodes, Inc.	1	0.36	0.36
250 V SP	Metal Oxide Varistors	Harris Semiconductor	2	0.39	0.78
1 kΩ, 200 W	Power Resistor	Huntington Electric, Inc.	1	10.30	10.30
40 kΩ, 1 W	Power Resistor	XICON	1	0.13	0.13
4 kΩ, 10 W	Power Resistor	Ohmite	1	1.73	1.73
100 Ω, 1 W	Power Resistor	XICON	2	0.14	0.28
0.01 Ω	Current Sensing Resistor	Ohmite	2	0.39	0.78
10 Ω, ¼ W	Resistor	Yageo	2	0.05	0.10
1 kΩ, ¼ W	Resistor	Yageo	19	0.05	0.95
4.99 kΩ, ¼ W	Resistor	Yageo	1	0.05	0.05
5.6 kΩ, ¼ W	Resistor	Yageo	1	0.05	0.05
10 kΩ, ¼ W	Resistor	Yageo	5	0.05	0.25
20 kΩ, ¼ W	Resistor	Yageo	1	0.05	0.05
39 kΩ, ¼ W	Resistor	Yageo	1	0.05	0.05
47 kΩ, ¼ W	Resistor	Yageo	2	0.05	0.10
90.9 kΩ, ¼ W	Resistor	Yageo	2	0.05	0.10
100 kΩ, ¼ W	Resistor	Yageo	8	0.05	0.40
120 kΩ, ¼ W	Resistor	Yageo	1	0.05	0.05
500 Ω, ½ W	Potentiometer	Bourns	2	1.20	2.40
1 kΩ, ½ W	Potentiometer	Bourns	2	0.88	1.76
1 kΩ, 5 W	Linear Taper	XICON	1	3.31	3.31
Knob	Speed Pot Knob	Kilo International	1	5.18	5.18
Total Components			91	Total Prototype Cost	104.42

Appendix B – Converter Wiring Diagram

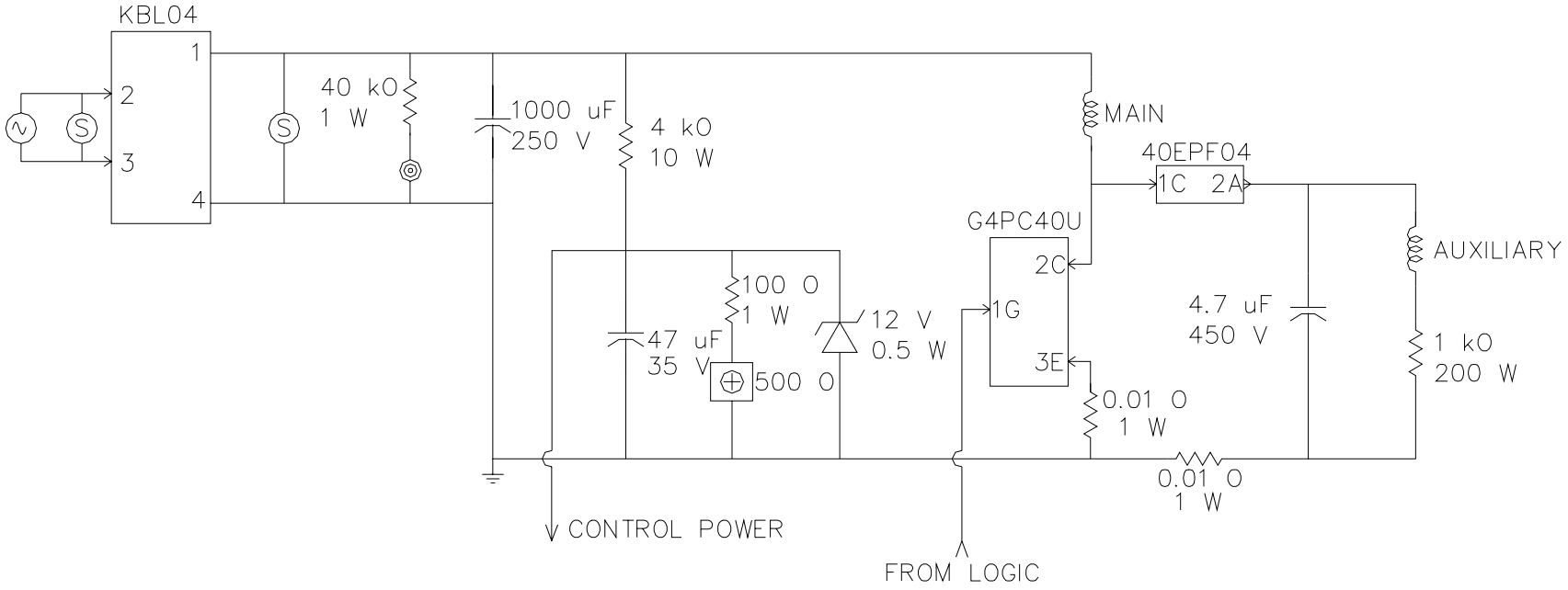

Appendix C – Current Control Loop Logical Schematic

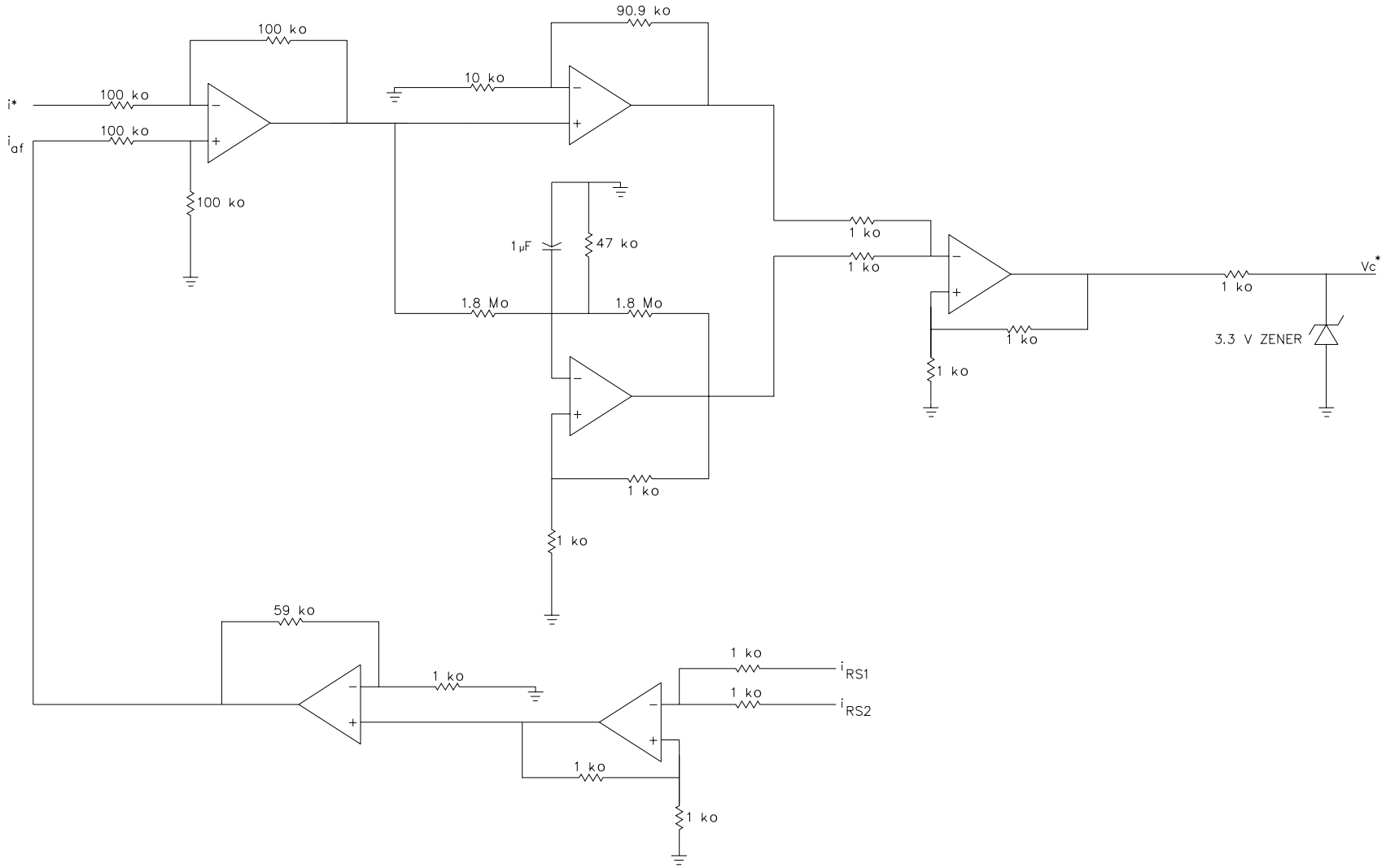

Appendix D – Current Control Loop Wiring Schematic

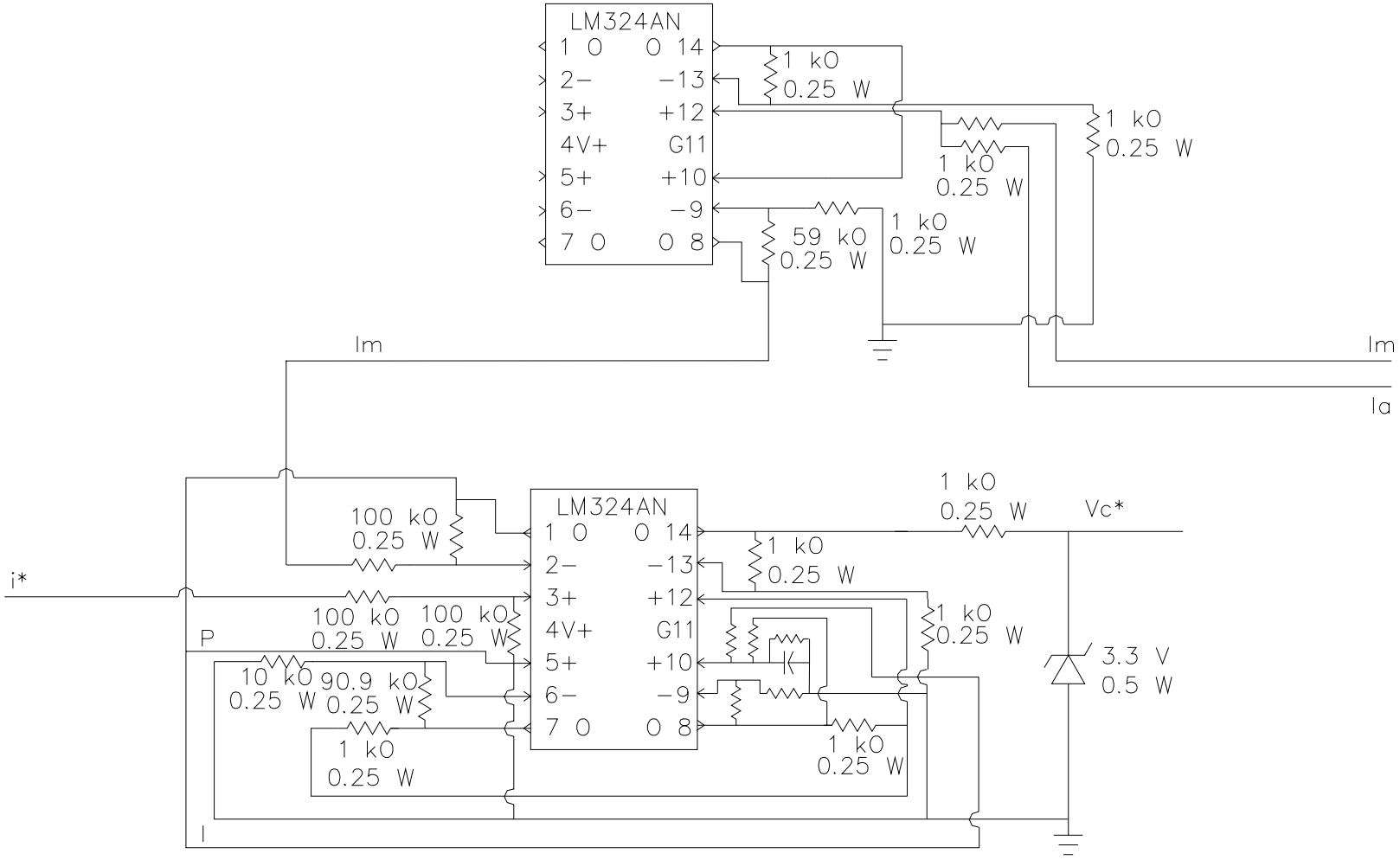

Appendix E – Speed Control Loop Logical Schematic

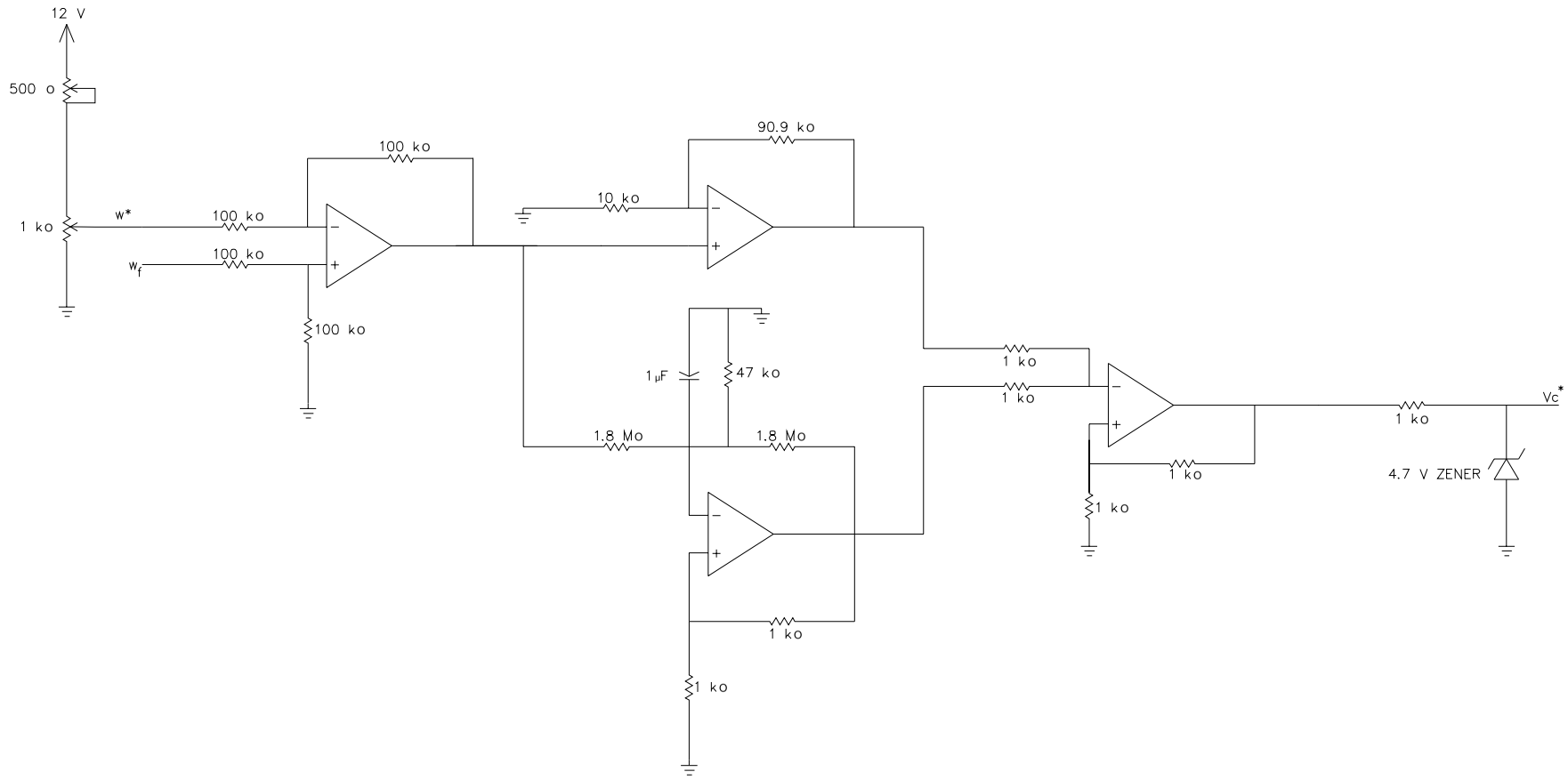

Appendix F – Speed Control Loop Wiring Schematic

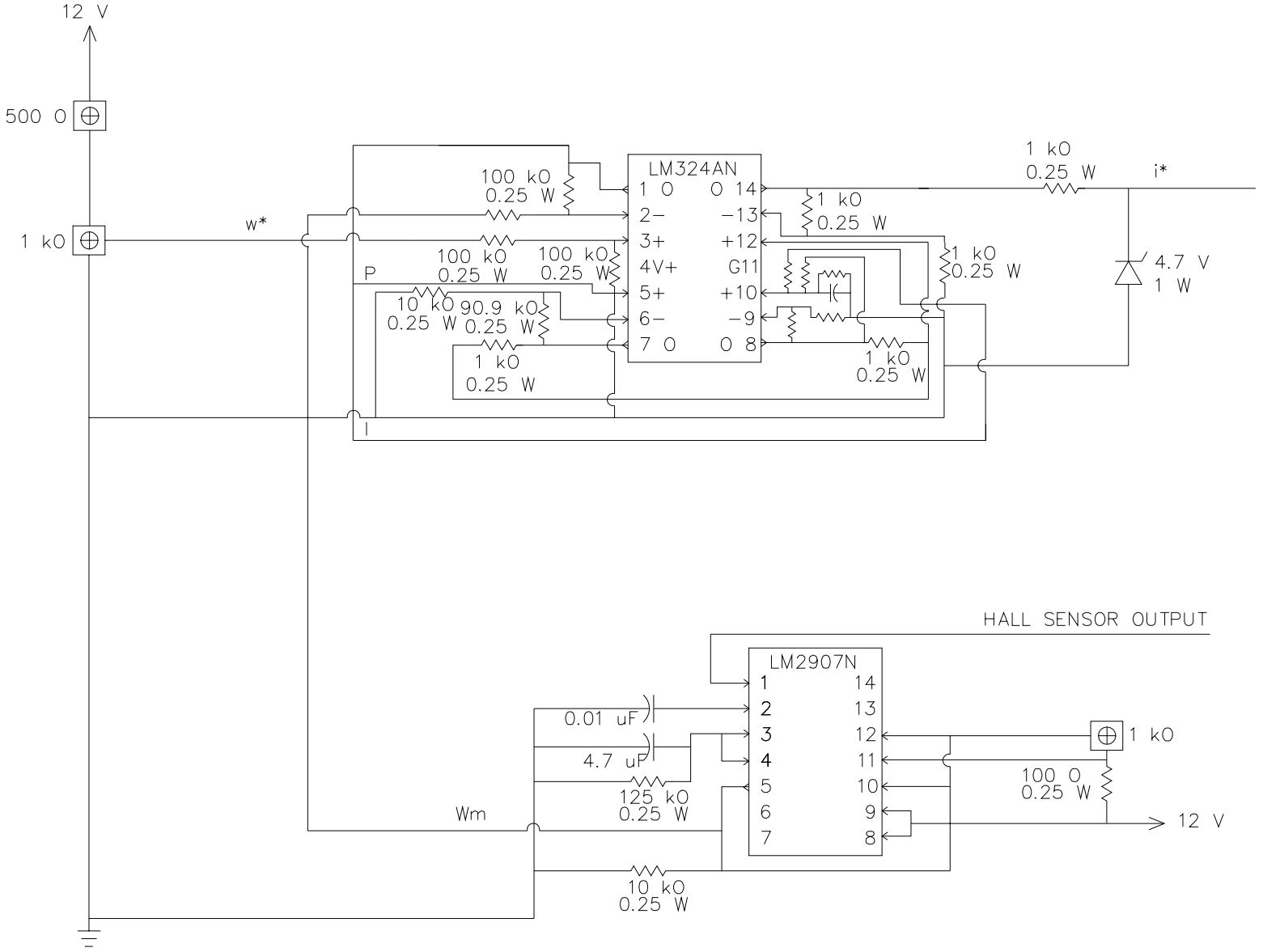

Appendix G – Total System Wiring Diagram

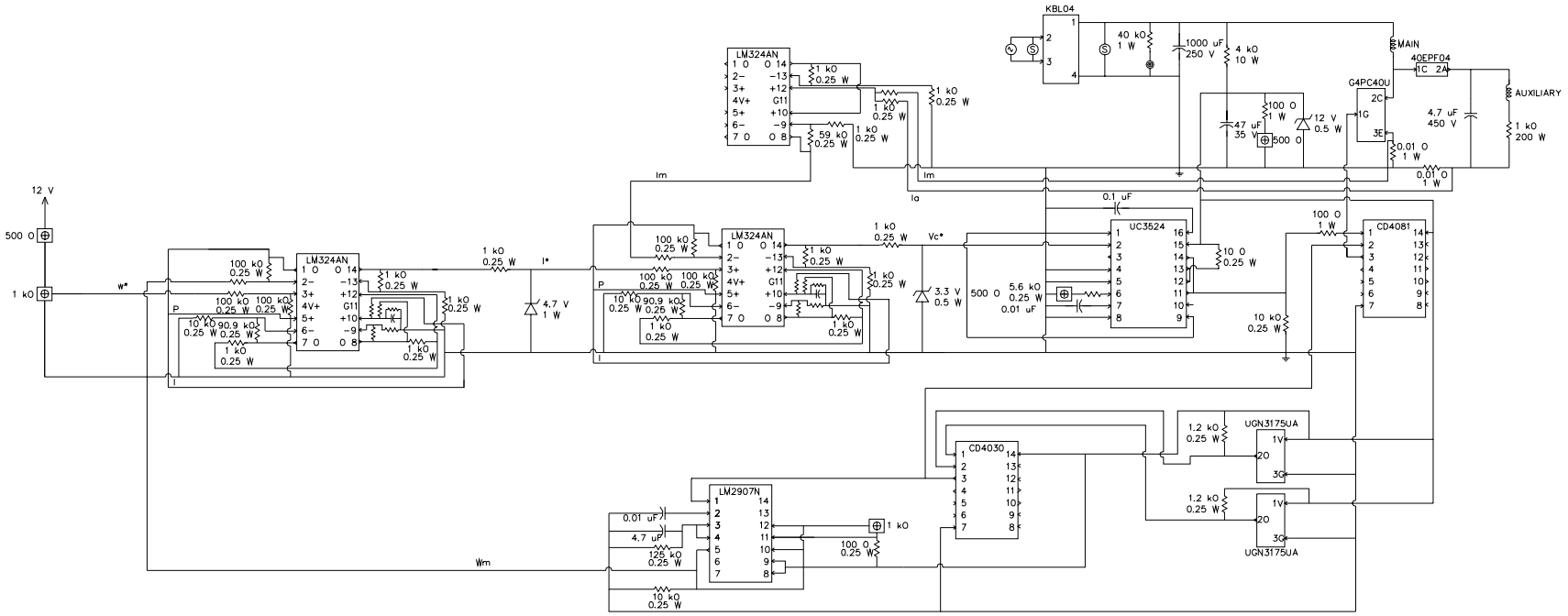

Vita

Amanda Martin Staley was born Amanda Christine Martin on February 8, 1978 in Richmond, Virginia to Charles David and Brenda Jean Martin. She graduated with honors from Monacan High School in Chesterfield County, Virginia in June of 1995. During her undergraduate years, she interned with Philip Morris USA (Cigarette Manufacturing Division) in Richmond, Virginia as an electrical engineer in the manufacturing and technical support divisions. Also, she interned with Delta Airport Consultants, Inc. (Airport Design Consulting Firm) as an electrical design engineer. She was named a Bradley Scholar in May of 1996 in the Bradley Department of Electrical and Computer Engineering. She graduated Magna Cum Laude as a Commonwealth Scholar from Virginia Polytechnic Institute and State University in May of 1999 with a Bachelor of Science in Electrical Engineering. She earned her Engineer-In-Training (E.I.T.) certification in June of 1999. She was named a Bradley Fellow in May of 1999 in the Bradley Department of Electrical and Computer Engineering. After the completion of her master's degree, she will pursue her Ph.D. in Electrical Engineering at Virginia Polytechnic Institute and State University as a Bradley Fellow. Her research interests include: single-phase switched reluctance motor drives, single-phase brushless DC drives, motor topology design, and industrial control systems.